Evidence for three interacting potential energy surfaces in the photodissociation of ICN at 249 nm

J. F. Black, J. R. Waldeck,[a] and R. N. Zare[b]
Department of Chemistry, Stanford University, Stanford, California 94305

(Received 10 November 1989; accepted 12 December 1989)

Cyanogen iodide (ICN) is photodissociated at 249 nm. The CN $X\,^2\Sigma^+$ photofragment is probed by sub-Doppler laser-induced fluorescence (LIF), allowing the extraction of recoil velocity anisotropies and branching ratios to the two iodine atom spin–orbit states $I(^2P_{1/2})$ and $I(^2P_{3/2})$ as a function of the CN ($v=0$) rotational state. The quantum yield for $I(^2P_{1/2})$ production Φ_{I^*} is found to be $43\% \pm 3\%$, in excellent agreement with the recent diode laser spectroscopic measurement of Hess and Leone. The population of the F_1 and F_2 spin–rotation doublet components shows nonstatistical behavior over a wide range of N for *both* I atom spin–orbit state exit channels. The results suggest that trajectories leading to $I(^2P_{1/2})$ evolve on an essentially collinear surface; the CN fragments being found in low rotational levels with almost limiting values of the system anisotropy parameter ($\beta = 1.85$ to 1.9). This value of β yields an estimate for the dissociative lifetime [$CN\,X\,^2\Sigma^+\ v=0, N=0; I(^2P_{1/2})$] of 90 ± 15 fs at this photolysis wavelength. There is evidence that trajectories leading to $I(^2P_{1/2}) + CN(v=0)$ in intermediate N levels have sampled a bent surface, indicating that multiple curve crossings occur in this channel. The nature of trajectories correlated to $I(^2P_{3/2})$ is very complicated, with clear evidence for a mixed parallel and perpendicular initial transition and subsequent curve crossings. The CN ($v=0$) fragments formed in conjunction with this channel are found predominantly in medium to high rotational quantum states. The system anisotropy parameters vary as a function of N, being negative at low N and becoming positive at high N. An analysis of the correlation between fragment velocity and rotation yields results inconsistent with a pure parallel or perpendicular excitation. We present a model involving three interacting surfaces, by which we can reconcile all major experimental observations at this photolysis wavelength.

I. INTRODUCTION

Certain small molecules continue to serve as benchmark systems for the development of photodissociation experiments and the understanding of photodissociation dynamics.[1–6] Of these, the photodissociation of ICN in the first absorption band, the "$\tilde{A}$ continuum," remains one of the most highly studied contemporary systems.[7–41] Theoretical interest in ICN stems from a number of factors.[7–19] First of all, we note the potential simplicity of the dissociation of a triatomic molecule whose fragments are theoretically quite tractable. Secondly, the ICN $\tilde{A}$ continuum is believed to be primarily a linear–linear transition, so that the resulting dynamics can be easily visualized in three dimensions. Finally, the large spin–orbit interaction of the iodine atom presents a number of subtle and intriguing complications involving curve crossings and other nonadiabatic interactions in the photodissociation dynamics.

ICN is also appealing from an experimental point of view.[20–41] It is easy to handle, has an absorption band in a region of the electromagnetic spectrum readily accessed by current laser systems, and yields photolysis products (I and CN) that are also easily probed by a large variety of laser-based diagnostic techniques.

Despite many experimental studies performed on this system, the photodissociation dynamics remain poorly understood. The most glaring and fundamental gap in our knowledge concerns the numbers and symmetries of the electronic states comprising the $\tilde{A}$ continuum. Moreover, there is persuasive evidence that the time evolution of the dynamics on these surfaces cannot be discussed in a separated, adiabatic formalism and that it is necessary to consider the coupling of these surfaces.

Various salient features emerge from previous experimental studies of this system. The work of Ling and Wilson[21] and Nadler *et al.*[31] indicates that, for 266 nm photolysis, the fragments are produced from electronic transition(s) of essentially "parallel" character with subsequent rapid dissociation. The work of Fisher *et al.*,[26] Marinelli *et al.*,[29] and O'Halloran *et al.*,[37] analyzing the rotational distributions of the CN (X,v) fragment, indicates highly nonstatistical population distributions, even to the extent that, for increasing CN vibrational quantum number v, the average N for the v formed also increases. The work of Hall *et al.*[32] and O'Halloran *et al.*[37] shows that the alignment of the CN fragment (defined as $A_0^{(2)} \equiv \langle (3J_z^2 - \mathbf{J}^2)/\mathbf{J}^2 \rangle$, proportional to $P_2(\hat{J}\cdot\hat{Z})$), changes as a function of N, being large and negative at low N and tending to 0 for increasing N.

Pitts and Baronavski,[23] and Hess and Leone[36] have performed thorough studies of the I*/I branching ratio as a function of photolysis wavelength. Their results show that I* production peaks at $\sim$260 nm with the I channel favored to longer and shorter wavelengths. At 249 nm Hess and Leone find that the I* quantum yield is $44.0\% \pm 4\%$.

Since the work of Shokoohi *et al.*[30] in 1984, considerable

[a] Present address: Chemistry Department, University of Pittsburgh, Pittsburgh, PA 15260.
[b] Author to whom correspondence should be addressed.

 0021-9606/90/063519-20$03.00

attention has been paid to a peculiar feature of this type of system, namely, the nonstatistical population of the F_1 and F_2 spin–rotation components in the CN ($X^2\Sigma^+$) fragment.[30,31,35,41] Recent theory[35] would suggest that this is a manifestation of nonadiabatic processes occurring during the dissociation and we will present further evidence of these effects.

Recently, two advances in the experimental study of the ICN $\tilde{A}$-continuum photodissociation dynamics have been made. Firstly, the advent of subpicosecond[33,40,42] laser pulses has enabled Zewail and co-workers to monitor the dissociation dynamics in essentially "real time." They have measured the CN build-up periods and perturbation-shifted resonances of CN as the fragments separate, in a technologically demanding series of experiments. The results of these and other femtosecond time-resolved studies have been reviewed recently by Zewail.[43]

Secondly, we call attention to the work of Hasselbrink *et al.*,[39] who photodissociated ICN at 249 nm using circularly polarized light. By using a circularly polarized probe laser they were able to measure the *orientation* [proportional to $P_1(\hat{J}\cdot\hat{Z})$] of the CN ($X^2\Sigma^+, v, N$) fragments. The sign and trends of the $A_0^{(1)}$ moment as a function of N were found to resemble closely the N-dependent branching ratio I*/I of Nadler *et al.*[31] Sub-Doppler probing of the orientation as a function of N by Hasselbrink *et al.*[39] and subsequently by Black *et al.*[44] has unambiguously correlated the sign of orientation with the spin–orbit state of the iodine atom. A model incorporating nonadiabatic coupling between two potential energy surfaces has been proposed by Vigué *et al.*[17] to account for the observed trends in fragment orientation.

The motivation for the present work stems from our desire to uncover definitive evidence for nonadiabatic interactions between proximate surfaces in the photodissociation dynamics of ICN. For this purpose, we have recorded Doppler profiles of the CN ($v = 0$) fragment in various rotational states to extract scalar and vector properties. This study constitutes an extension of the work of Nadler *et al.*[31] to a different photolysis wavelength. We obtain the I*/I branching ratios, the F_1/F_2 population ratios, and the recoil velocity anisotropies for the CN ($X, v = 0$) fragments as a function of N. From an analysis of the combined data, we demonstrate the involvement of at least three different potential energy surfaces, two that correlate to the I($^2P_{3/2}$) asymptote, one to the I($^2P_{1/2}$) asymptote. This leads to a picture for the photodissociation dynamics of ICN much richer than previously surmised.

II. EXPERIMENTAL

Figure 1 shows schematically the apparatus, which is a standard crossed-geometry LIF cell, described previously.[35,37,39] The photolysis light was provided by a Lumonics TE 861-2 laser operating on the KrF exciplex transition [$\sim$249 nm, 200 mJ per pulse, $\sim$15 ns full width at half-maximum (FWHM)]. A Lambda Physik FL2002E dye laser was pumped by a portion (50%) of the photolysis laser output. This provided tunable radiation around 358 nm (PBD dye in cyclohexane, Exciton) with a bandwidth of $\sim$0.12 cm^{-1}, which could be narrowed to $\leqslant$0.06 cm^{-1} using an intracavity etalon. Only the oscillator/preamplifier stage was used.

The photolysis beam was recollimated using an $f = 1000$ mm lens, irised down to a circular spot of $\sim$8 mm diameter and passed through CaF_2 polarizing elements to provide a highly polarized source (extinction ratios $>$200:1). The beam was then passed through a second lens ($f = 300$ mm) to correct for residual divergence and sent into the cell via extensively baffled arms. The entrance and exit windows of these arms were purged with a low pressure of argon (10 mTorr) to reduce absorption of the light in the arms by the ICN and to counter the buildup of photolysis product debris on the windows, which was found to attenuate severely the incoming UV over a period of a few days. The pulse energies of the 249 nm beam in the interaction region were kept to $\sim$800–900 μJ per pulse at the start of an experimental run. The inevitable decay of the excimer gas fill throughout the course of experimental runs ($\sim$8 h to 50% power) meant that the power could never exceed the initial conditions. Extensive checks revealed that the product intensities behaved in an entirely linear manner with respect to photolysis power in this regime. The measurements of the effective system anisotropy parameters were unaffected by random power fluctuations in experiments where the pulse energies were below 1 mJ.[45] The photolysis laser power was monitored on a shot-to-shot basis by a photodiode (Hamamatsu S1336-5BQ) coupled to a sample-and-hold circuit built in-house.

The CN $X^2\Sigma^+$ photofragments were monitored by LIF via the well-known CN $B^2\Sigma^+$–$X^2\Sigma^+$ band system.[46–51] Following the work of O'Halloran *et al.*,[37] we pump the B–X (1,0) transition and observe the B–X (1,1) fluorescence through an interference filter (Omega Optical) centered at 384 nm on the $\Delta v = 0$ sequence. Despite the less favorable Franck–Condon factors governing this transition,[48] pulses of 100–400 nJ were found to give good signal to noise in all cases. This is at least a factor of 30 below any calculated saturation threshold. The intensities and shapes of the rotational lines behaved in an entirely linear, predictable manner with respect to probe laser power. Absolute powers were measured with a Molectron J3 power monitor and shot-to-shot assessment was made by monitoring the output of a photodiode (Hamamatsu S1336-5BQ). All data were normalized linearly to the photolysis and probe laser powers.

The dye laser beam was passed round an optical delay line to give $\sim$35 ns delay between pump and probe pulses. The beam was sent through polarizing elements to give a well-defined probe polarization (extinction ratios $>$250:1) and then propagated through the cell via extensively baffled arms. No purge was applied to the dye laser arms. The walls of the interaction volume of the cell were coated with matt black paint (Zuel Corporation, St. Paul, MN) to reduce scattered light. This is superior to graphite spray coating, which seems to fluoresce when excited at 249 nm.

The dye laser beam was also monitored by two external etalon assemblies. One provided a simple fringe pattern that was monitored by a photodiode (Hamamatsu S1336-5BQ) and provided a wavelength calibration for all the spectra. A

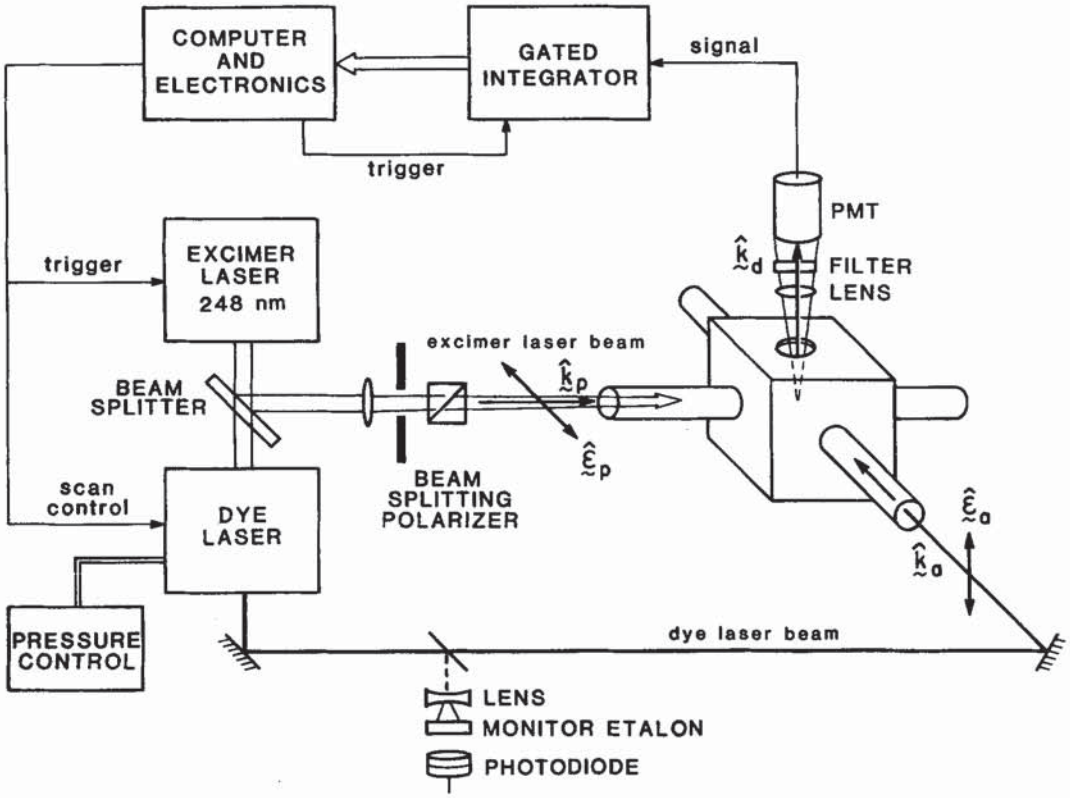

FIG. 1. A schematic diagram of the apparatus used in the CN Doppler profile studies following photolysis of ICN. Note the arrangement of the wave vectors and electric vectors of the photon fields.

second produced the image of a fringe pattern on a Reticon diode array (EG&G) that was continuously monitored on an oscilloscope. This was invaluable for initial setup of the dye laser and real-time monitoring of the mode quality of the dye laser output. The dye laser was pressure tuned (using dry, filtered nitrogen).

ICN (Kodak) flowed as a vapor through the chamber at pressures of 2–10 mTorr. The ICN was sublimated *in vacuo* prior to an experiment and kept in a darkened container; no evidence for impurities or memory effects from previous laser pulses was ever observed. At the total pressures of ICN and Ar used, the spectra were taken under conditions representing less than one-tenth of a gas kinetic cross-section collision per unit delay time interval, assuming the CN has the maximum velocity allowed given the energetics of the system (~ 3.2 km s^{-1}). As we shall see, this represents a conservative upper limit on collisional quenching because most CN fragments are moving much more slowly.

LIF photons were detected along the direction normal to the plane containing the wave vectors of the pump and probe radiation. The key point here (Fig. 1) is that the dye laser beam propagated parallel to the electric vector of the photolysis laser beam. As already shown by Nadler *et al.*,[31] there is little useful information in geometries where the dye laser beam propagates perpendicular to the axis of cylindrical symmetry, defined by ϵ_p; in any case, these geometries are more severely affected by vector correlations.[52–56] Rotating the dye laser polarization (such that it lies either in the plane defined by the wave vectors of the pump and probe lasers or normal to it) changed the appearance of the spectra somewhat because of the correlation of photofragment angular momentum distribution and angular recoil velocity distribution.[57]

A single lens (1.5 in diameter; $f = 60$ mm) in the vacuum collected the fluorescence and focused it onto the photocathode of the photomultiplier tube (RCA 7326) operated at 1700 V. The anode was connected directly to the input of a $\times 10$ preamplifier (Le Croy VV100BTB) and the single output was fed into a boxcar integrator (SRS 250). The LIF signal was integrated for 120 ns (about two lifetimes[46]) and was captured on a shot-to-shot basis by a laboratory microcomputer that also stored the monitor etalon data and power diode signals. The averaged output of the boxcar was sent to a chart recorder for real-time monitoring of the experiment. All the computer analog-to-digital (A/D) converters were operated in a linear response regime, and extensive checks were made to preserve the 50 Ω impedence characteristics of all signal circuitry and the faithfulness of the electronics in general. An external trigger provided the fire command for the laser and synchronization of the boxcar, sample and hold, and A/D circuits.

III. RESULTS

A. Doppler profiles

Figure 2 shows a typical broadband (no etalon) scan of the CN B–X (1,0) band over the region 353.05–352.50 nm taken under the conditions described above. Clearly visible is the (1,0) progression, the minor features being progressions in the (2,1) and (3,2) bands. The structure on the lines

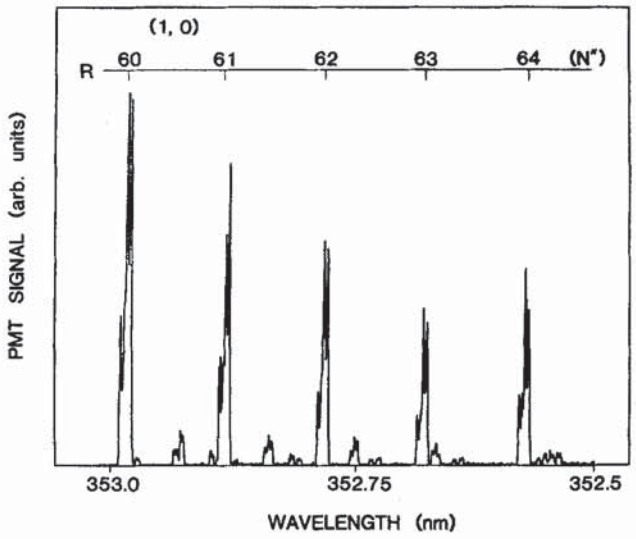

FIG. 2. Laser-induced fluorescence signal in the short wavelength tail of the CN $B\,^2\Sigma^+ - X\,^2\Sigma^+$ (1,0) band. Minor features are lines in the (2,1) and (3,2) bands.

is caused by a combination of two factors. First, spin–rotation interaction causes the F_1 and F_2 components to be resolved, especially at high N. Second, each F_1 and F_2 transition is split by the recoil velocity of the fragment, yielding large Doppler shifts. This is observable because of the particular viewing geometry employed.

We have studied lines in the CN B–X (1,0) band that are uncontaminated by accidental coincidences with lines of the underlying (2,1) and (3,2) bands. The Franck–Condon factors for the (2,1) and (3,2) bands[48] cause a disproportionately large LIF signal with respect to their actual populations, relative to the (1,0) band.

Figures 3–11[58] show the LIF spectra of representative R branch lines, probed as described with $\mathbf{k}_a \| \boldsymbol{\epsilon}_p$ and $\mathbf{k}_d \| \boldsymbol{\epsilon}_a$.

The profiles shown have been normalized to unit area. Each profile entailed a scan time of about 15–20 min. Day-to-day repetition of line profiles showed no correlated discrepancies. Immediately obvious in Fig. 3, the $R(0)$ line profile, is the large Doppler broadening and extreme laboratory frame anisotropy of recoil velocity. The solid line is the result of a fit to be described later. The residuals from this fit are shown in the panel beneath the profile. Figures 4–11 show the development of the Doppler-broadened profiles as N increases for the CN ($v = 0$) fragment. Spin–rotation doubling is clearly visible in Figs. 10 and 11, as is the nonstatistical population of these states—now a well-known feature of this type of photodissociation.[30,31,35,41]

B. Analysis of Doppler profiles

A number of authors have theoretically treated the angular distribution of photofragments to various levels of sophistication.[59–70] As a starting point, we have[59,60]

$$I(\theta) = \frac{1}{4\pi}\,(1 + \beta P_2(\cos\theta)), \tag{1}$$

where $I(\theta)$ is the doubly differential cross section for photofragments scattering into a solid angle $\sin\theta\, d\theta\, d\phi$, and where θ is defined as the angle between the photolysis beam electric vector $\boldsymbol{\epsilon}_p$ and the recoil velocity vector $\mathbf{v}$. Equation (1) has azimuthal symmetry. β is the so-called anisotropy parameter (dimensionless) and $P_2(\cos\theta)$ is the second Le-

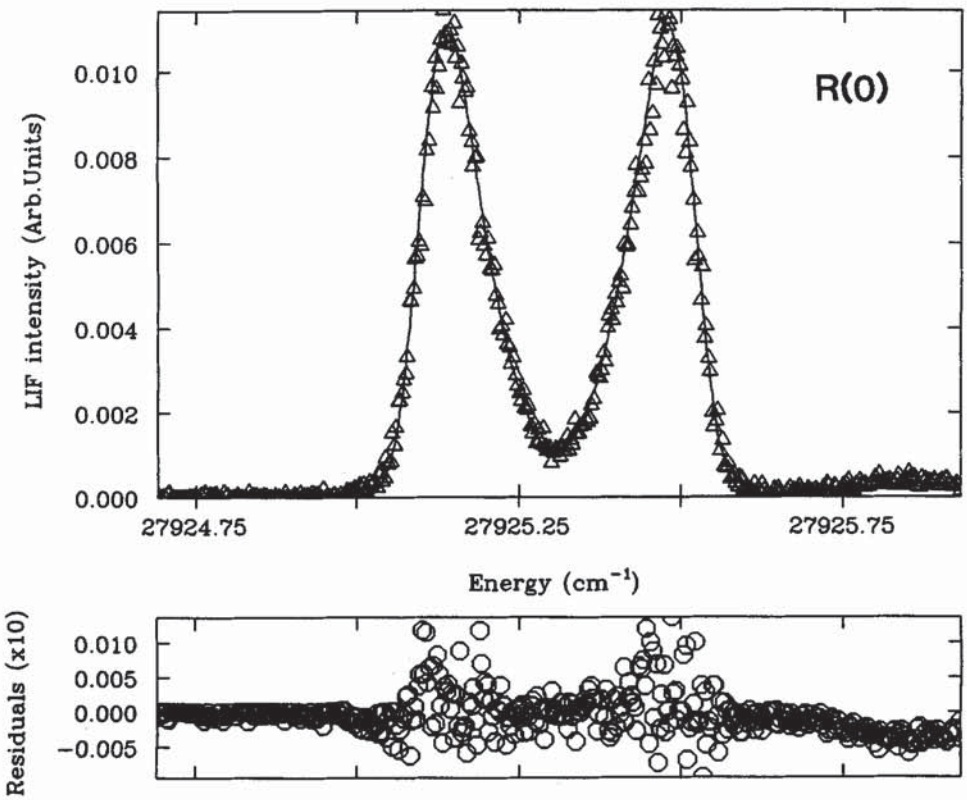

FIG. 3. High-resolution fluorescence excitation spectrum of the $R(0)$ line of the CN B–X (1,0) band. Solid line is a fit to the data (triangles). Residuals from the fit (circles) are shown in the lower panel, plotted at a scale $\times 10$ of that of the main spectrum.

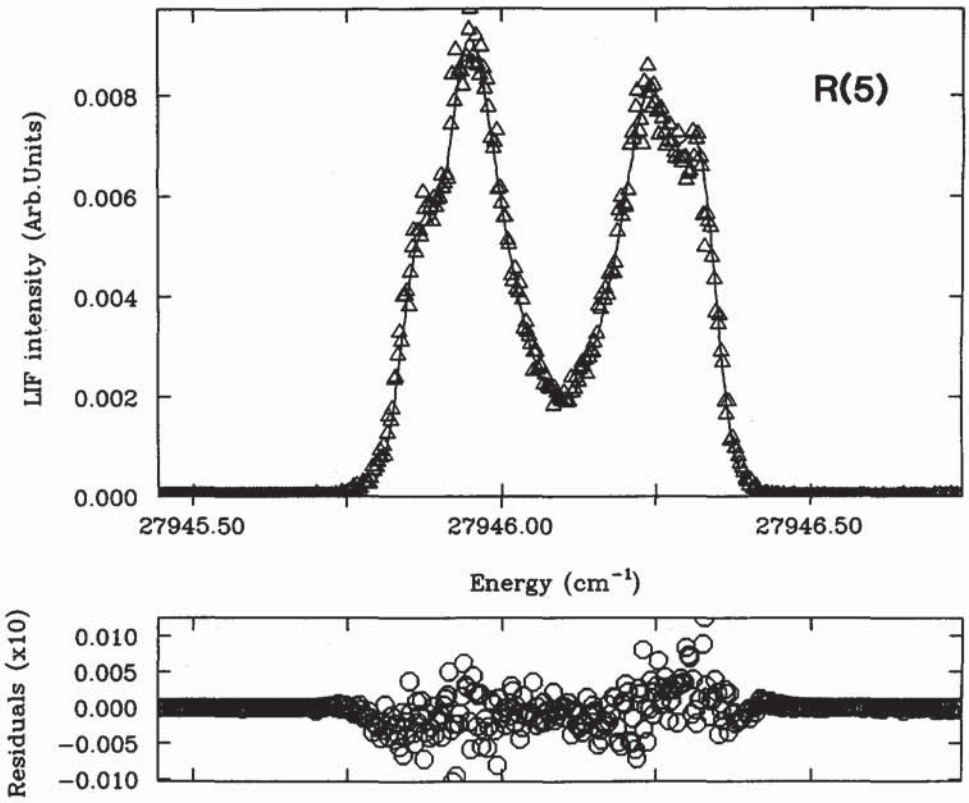

FIG. 4. High-resolution fluorescence excitation spectrum of the $R(5)$ line (see Fig. 3).

gendre polynomial in $\cos\theta$. Classically, the β parameter may be further decomposed as[66]

$$\beta = 2P_2(\cos\chi)P_2(\cos\alpha)g(\omega,t) \tag{2}$$

for linear molecules, where χ reflects the symmetry of the transition ($\chi = 0°$ for a parallel transition and $\chi = 90°$ for a perpendicular transition), α is the angle through which the parent molecule rotates prior to the fragments separating to beyond the limit of mutual interaction (see, e.g., Figs. 3 and 5 of Ref. 70), and $g(\omega,t)$ is a function describing the effect

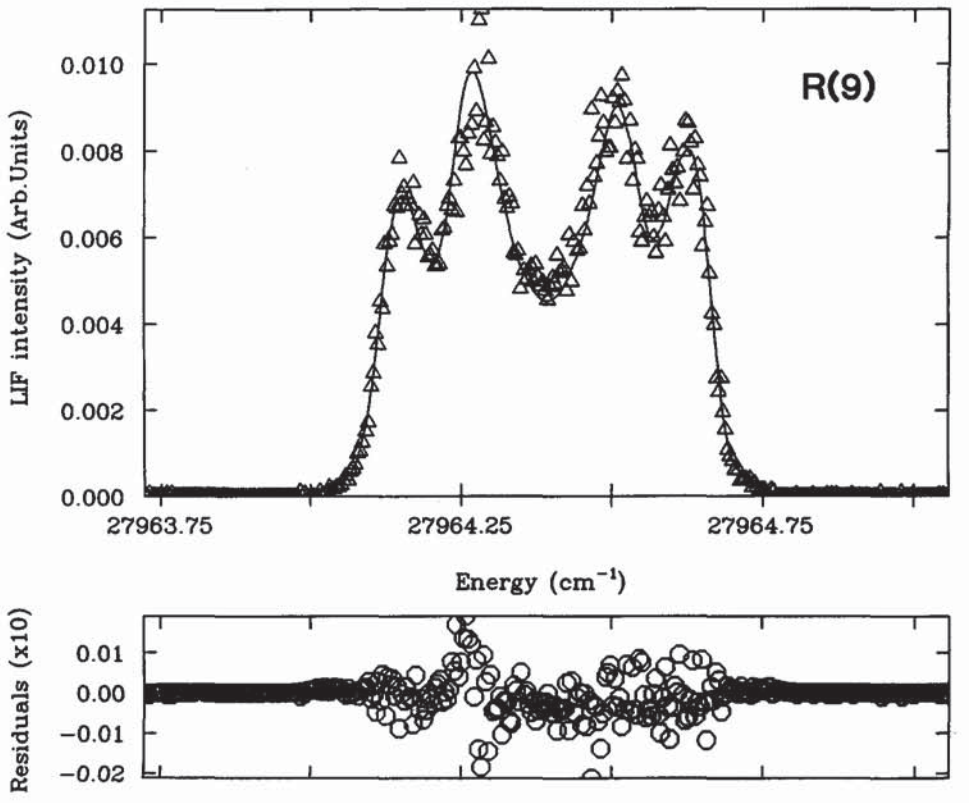

FIG. 5. High-resolution fluorescence excitation spectrum of the $R(9)$ line (see Fig. 3).

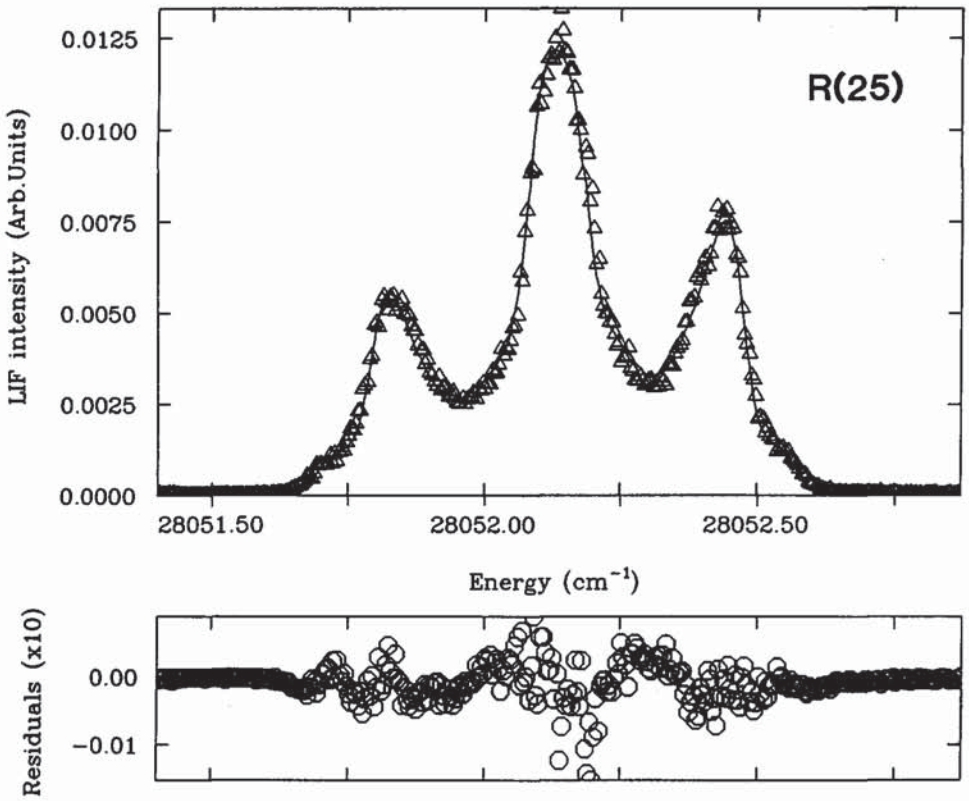

FIG. 6. High-resolution fluorescence excitation spectrum of the $R(25)$ line (see Fig. 3).

of dissociation lifetime on the angular distribution caused by molecular rotation. For a linear molecule[63]

$$g(\omega,t) = \frac{1+(\omega\tau)^2}{1+4(\omega\tau)^2}, \tag{3}$$

where ω is the angular velocity of separation. Averaged over a Boltzmann distribution of rotation, Eq. (2) becomes [67]

$$\beta = \frac{1}{2} P_2(\cos\chi)\left\{1 + 3\gamma e^{\gamma}\int_{\gamma}^{\infty} e^{-v}\frac{dv}{v}\right\}, \tag{4}$$

where

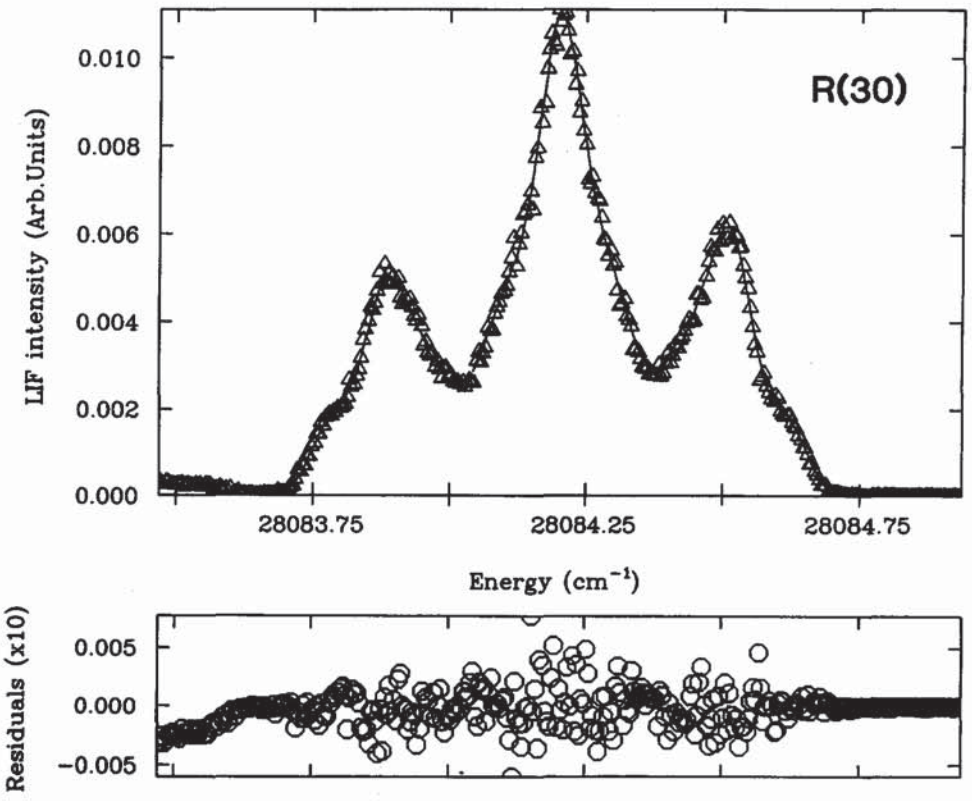

FIG. 7. High-resolution fluorescence excitation spectrum of the $R(30)$ line (see Fig. 3).

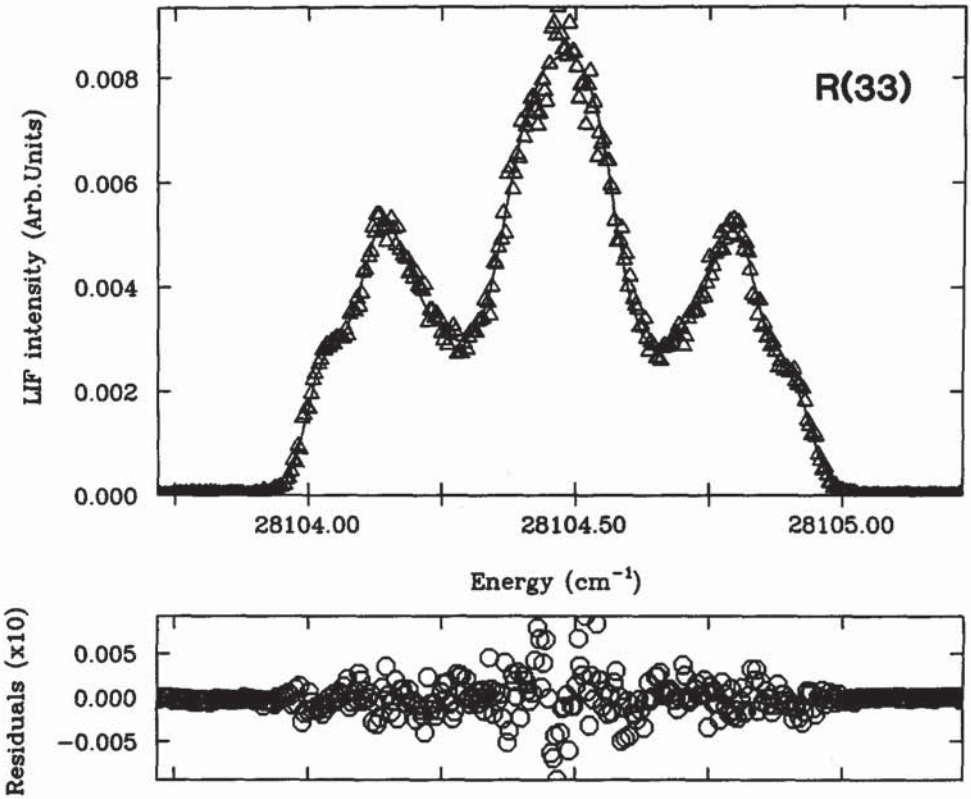

FIG. 8. High-resolution fluorescence excitation spectrum of the $R(33)$ line (see Fig. 3).

$$\gamma = I/8kT\tau^2, \tag{5}$$

I is the moment of inertia of the parent molecule, and τ is the average dissociation lifetime. This gives, in the limit of fast dissociation,

$$-1 \leqslant \beta \leqslant 2, \tag{6a}$$

and for slow dissociation,

$$-\tfrac{1}{4} \leqslant \beta \leqslant \tfrac{1}{2}. \tag{6b}$$

More detailed treatments of the effects of lifetime and parent rotation can be found in Nagata *et al.*[64] and Jonah.[63]

We see that the β parameter itself is a product of various antagonistic mathematical functions. Its predictive or interpretive value is therefore limited, but as it approaches the

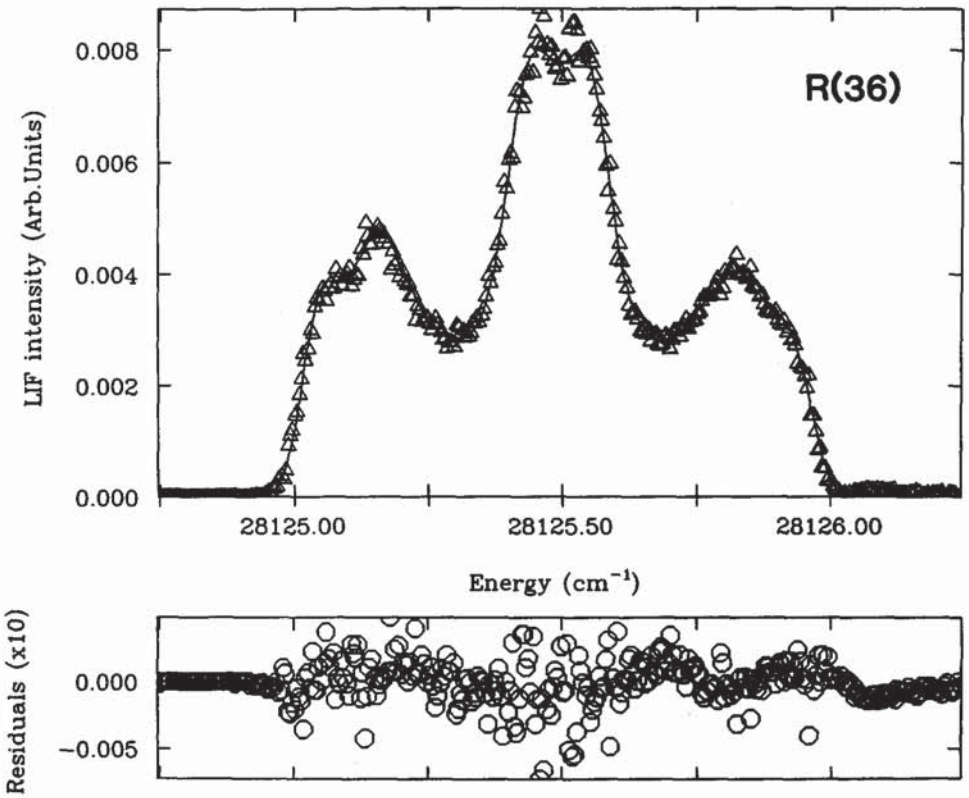

FIG. 9. High-resolution fluorescence excitation spectrum of the $R(36)$ line (see Fig. 3).

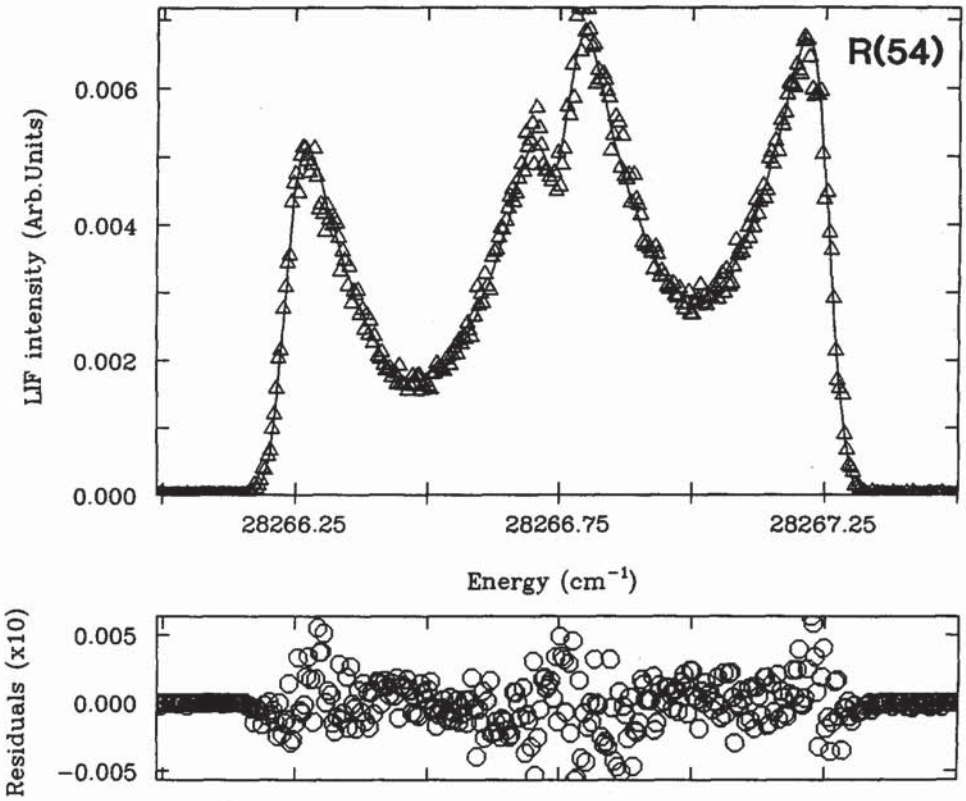

FIG. 10. High-resolution fluorescence excitation spectrum of the $R(54)$ line (see Fig. 3).

rapid dissociation limits it becomes more useful and some qualitative information may be obtained.

Consider an isotropic angular distribution of photofragments with some particular velocity $\mathbf{v}$. Probing the ensemble with LIF would yield, in the first instance, a rectangular profile with full width $(2\nu_0|\mathbf{v}|)/c$, where ν_0 is the natural, unshifted resonant absorption frequency and c is the speed of light. This is then convoluted with the finite laser bandwidth (usually approximated as a Gaussian) and the parent center-of-mass motion (again represented by a Gaussian). Let us include next the effects of an anisotropic recoil velocity distribution. Again for a single velocity $\mathbf{v}$, the detuning from

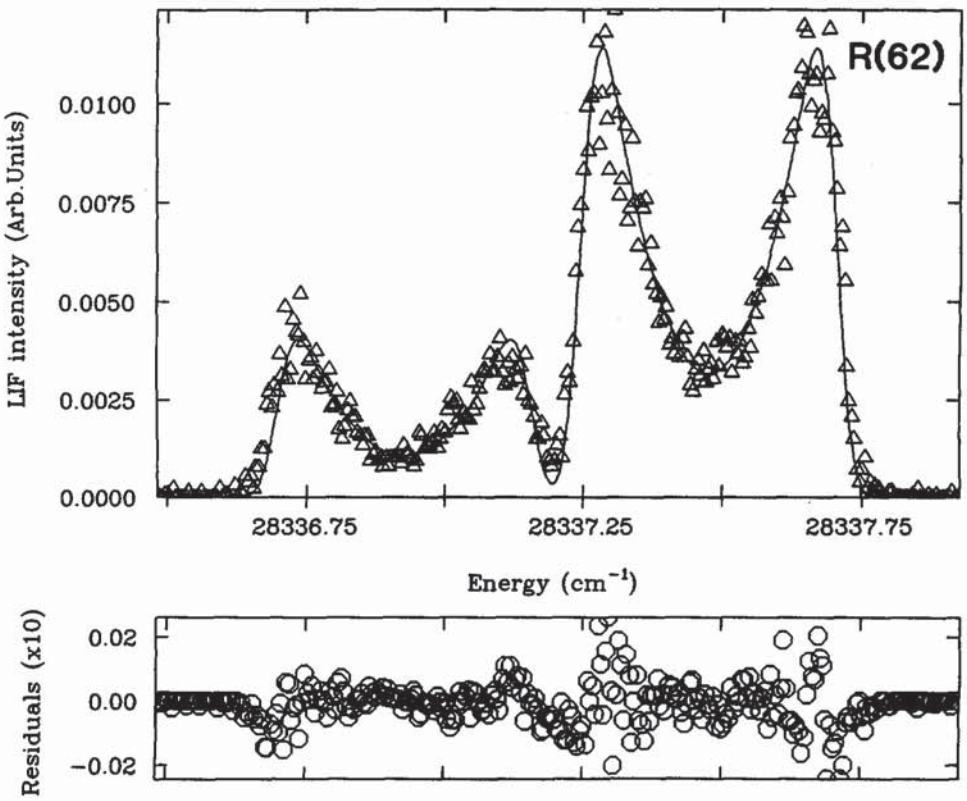

FIG. 11. High-resolution fluorescence excitation spectrum of the $R(62)$ line (see Fig. 3).

the line center ν_0 will be a function of the projection of the fragment recoil velocity on the propagation axis of the probe laser

$$|\mathbf{v}'| = |\mathbf{v}|\cos\theta, \tag{7}$$

where $\cos\theta = \mathbf{v}\cdot\mathbf{k}_a$. The appearance of the LIF transition (the "Doppler profile") is now described by an expression of the form (in frequency space)[31,52,54,56]

$$I(\nu) \propto \left[1 + \beta_{\text{eff}} P_2\left(\frac{c(\nu-\nu_0)}{\nu_0|\mathbf{v}|}\right)\right]. \tag{8}$$

We proceed from here with the notation β_{eff} (the effective system anisotropy parameter), signifying not only the implicit incorporation of the various factors described above, but also the further complicating influence of vector correlations (between the angular momentum distribution and angular recoil velocity distribution) on the parameters.[52–56] The effects of the latter constitute the critical difference between LIF and the more classical "integrating" techniques such as neutral time-of-flight (TOF) photofragment spectroscopy.[71–74] REMPI extensions of the TOF technique have been employed recently by a number of groups[75–78] to allow the study of these more subtle properties of photodissociation hitherto only accessible by LIF.[5]

Our analysis here is complicated by two features of the system. Firstly, we can produce the I atom partner in one of two spin–orbit states differing in energy by 7603 cm^{-1}. This will produce CN fragments, for a given N, with two distinct speeds and consequently two convoluted Doppler profiles. An unfortunate consequence of the energy-to-velocity mapping ($E = 1/2mv^2$) is that, for very large energy releases such as the case under consideration here, the velocity resolution (the critical parameter in Doppler LIF studies) is very poor. However, as can be seen in Figs. 6–9, some of our profiles do show "shoulders" and other structure not attributable to the underlying spectroscopy, and we can distinguish the two channels, following the lead of Nadler *et al.*[31]

Secondly, the B–X transition is $^2\Sigma^+ - {}^2\Sigma^+$ and consequently shows spin–rotation doubling of the lines into F_1 ($J = N + 1/2$) and F_2 ($J = N - 1/2$). The splitting is described spectroscopically as a polynomial expansion in N and can be accounted for precisely.

We fit the Doppler profile to the functional form

$$I(\nu) = \sum_{i=1}^{4} a_i\left[1 + b_i P_2\left(\frac{c(\nu-\nu_0)}{\nu_0|\mathbf{v}|}\right)\right], \tag{9}$$

where the a_i are "population" factors, correctly scaled for the relative velocities, and the b_i are the β_{eff} parameters. The sum ranges from 1 to 4 because of the four contributing channels, viz.,

$$\text{I}(^2P_{1/2})\swarrow^{F_1}_{F_2},$$
$$\text{I}(^2P_{3/2})\swarrow^{F_1}_{F_2}.$$

The speed $|\mathbf{v}|$ for a given CN ($v = 0,N$) + I($^2P_{1/2,3/2}$) half-collision pair is obtained as follows: Energy is conserved so that

$$\langle E_{\text{par}}\rangle + h\nu - D_0^0(\text{I}-\text{CN}) = E_{\text{available}} = E_{\text{int}}(\text{I}) + E_{\text{int}}(\text{CN}) + E_{\text{trans}}. \tag{10}$$

From the fitting procedure, we obtain $E_{\text{available}} \sim 14\,400 \pm 200\ \text{cm}^{-1}$, the error being comparable to the parent ICN energy available at 300 K ($\sim 360\ \text{cm}^{-1}$),[31] and the spread of photolysis energy using this very broad lasing transition ($\sim 150\ \text{cm}^{-1}$).

For each iodine atom spin–orbit channel, the speed of the CN ($v = 0,N$) fragment is then given by

$$|\mathbf{v}| = \left[\frac{2M_{\text{I}}(E_{\text{available}} - E_{\text{int}}(\text{I}) - E_{\text{int}}(\text{CN}))}{M_{\text{CN}}M_{\text{ICN}}}\right]^{1/2}. \tag{11}$$

The experimental spectrum is first set on an accurate energy abscissa by fitting the etalon fringes to a polynomial function that is then used to calculate the frequency interval of the data points. The absolute CN B–X (1,0) transition frequencies are calculated using the constants of Cerny *et al.*[50] (X state) and Ito *et al.*[51] (B state). Terms up to $[N(N+1)]^4$ are included in the calculation. This calculation also gives the internal rotational energy of each CN ($v = 0,N$). The polynomial is constructed as per Eq. (9) and convoluted with Gaussian representing the laser linewidth (determined from the etalon fringes for each spectrum) and the ICN parent motion (about 0.028 cm^{-1} FWHM). For lines where the spin–rotation components are reasonably well resolved ($N > 15$), nonlinear least-squares fitting is then used to minimize the function

$$I(\nu)_{\text{expt}} - \sum_{i=1}^{4} a_i\left[1 + b_i P_2\left(\frac{c(\nu-\nu_0)}{\nu_0|\mathbf{v}|}\right)\right] \tag{12}$$

to determine the best values of a_i and b_i in a least-squares sense.

The program was developed around the NAG routine E04FCF[79] performing Gauss–Newton minimization of the function.[80] The fit was unconstrained. This is superior to interactive simulation as it (a) eliminates subjectivity and preconceptions surrounding the data and (b) allows a realistic error treatment for the parameters.

For each N, between three and six spectra were analyzed. All numerical data to be reported are the standard-deviation-weighted means[81] of the fit parameters from these determinations. All errors are the square roots of the means of the variances of the fit parameters. We usually use 3σ, corresponding to $> 95\%$ confidence for all N. The variance/covariance correlation matrices for the fits show that, as might be intuitively expected, some of the fit variables are highly correlated. This, in general, seems to affect the determinations of the β_{eff} parameters more than the populations. Representative back simulations of the data are shown in Figs. 3–11 (solid line is the fit, triangles are the data). Residuals are plotted on a scale $\times 10$ of that of the main panels. For lines where the spin–rotation components are poorly resolved ($N \leqslant 15$), the fitting program rapidly developed fatal oscillations and we were reduced to interactive fitting. The quoted errors in the latter procedure represent the latitude for which *gross* deterioration of the fit was observed.

One final caveat as regards analysis needs to be mentioned. The $v = 1$ level of CN $B\,^2\Sigma^+$ state is severely perturbed by the $v = 11$ and 12 levels of the $A\,^2\Pi$ state. This causes eigenstates to shift position and, more importantly, the spin–rotation splitting to vary quite dramatically in a fashion correlated with the proximity of the $A\,^2\Pi$ levels. In all the fits described, the spin–rotation doubling constant of the upper state γ' has been adjusted to optimize the fit.[82] Note that varying this splitting has a different effect to altering the energy release in the dissociation. Altering γ' causes the F_1, F_2 components to coalesce/separate, while altering the energy release causes a broadening/narrowing of each peak. Large deviations from the value of Ito *et al.*[51] can be precisely attributed to crossing of $A\,^2\Pi$ levels, being particularly apparent around $N' = 46$.

C. I*/I ratio

Figure 12 shows the fractional I* quantum yield, defined as

$$\Phi_{I^*}(N) = \frac{I(^2P_{1/2},N)}{I(^2P_{3/2},N) + I(^2P_{1/2},N)}, \tag{13}$$

plotted as a function of N for the lines studied. We convert this information into fractional populations [Fig. 13(a)] by multiplying $\Phi_{I^*}(N)$ and its conjugate $1 - \Phi_{I^*}(N)$ by the normalized rotational population distribution [Fig. 13(b)] taken from O'Halloran *et al.*[37] We note that CN ($v = 0$) fragments in low N correlate predominantly (but not exclusively) with the $I(^2P_{1/2})$ channel and those in high N correlate to $I(^2P_{3/2})$. This picture is similar to Fig. 3 of Nadler *et al.*[31] The I*/I ratio becomes unity around $N = 26 \pm 2$. This value is very similar to that reported by Nadler *et al.* ($N = 27$), but this is merely coincidence because, as we shall show, the dynamics are radically different between photodissociation at 249 and 266 nm. The contribution from $I(^2P_{3/2})$ rises monotonically from 4% at $N = 0$ to 100% at $N \geqslant 44$.

The overall quantum yield for $I(^2P_{1/2})$ is

$$\langle \Phi_{I^*} \rangle = 43 \pm 3\%. \tag{14}$$

This is in excellent agreement with the determination of Hess and Leone,[36] who used diode laser gain vs absorption spectroscopy to obtain $\langle \Phi_{I^*} \rangle = 44\% \pm 4\%$.

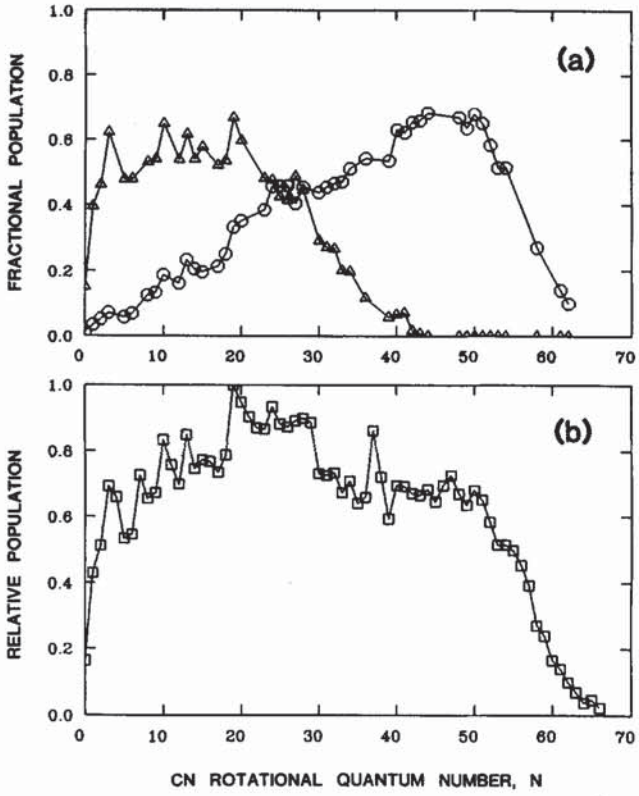

FIG. 13. (a) The CN rotational state distributions as a function of exit channel; △ correspond to $I(^2P_{1/2})$ and ○ to $I(^2P_{3/2})$. These plots are obtained by multiplying $\phi_{I^*}(N)$ or its conjugate $[1 - \phi_{I^*}(N)]$ with the relative population distribution of O'Halloran *et al.* (Ref. 37), which, for completeness, is reproduced in (b).

D. F_1/F_2 population ratios

Figure 14 shows a plot of the fine-structure difference function

$$f(N) = \frac{P(F_1) - P(F_2)}{P(F_1) + P(F_2)} \tag{15}$$

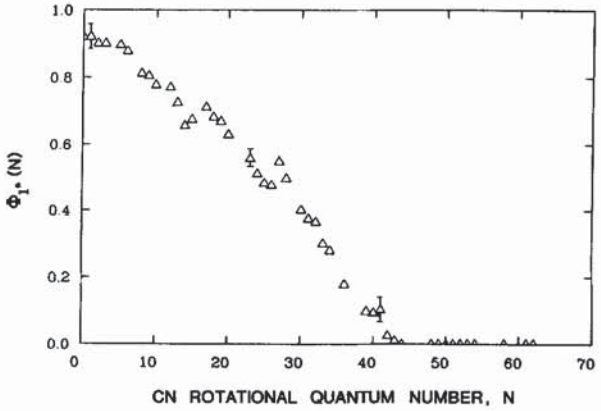

FIG. 12. The N-dependent I* quantum yield $\Phi_{I^*}(N)$ vs N for photolysis of ICN at 249 nm. Representative error bars (3σ) are indicated.

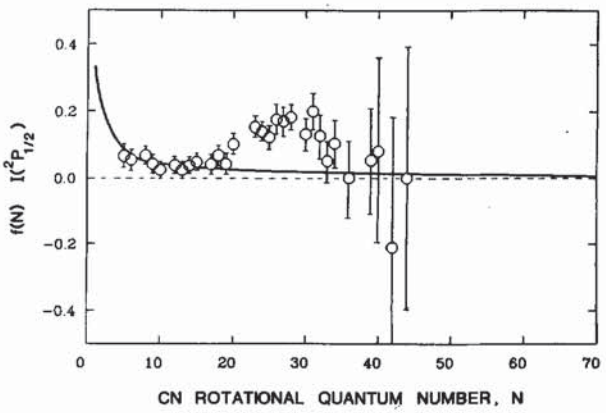

FIG. 14. The fine-structure difference function $f(N)$ vs N for photolysis yielding CN ($v = 0$) + $I(^2P_{1/2})$. Error bars (3σ) are obtained from those of the population analysis (Ref. 81). The solid line represents statistical behavior.

(as defined by Joswig *et al.*[35] for the CN ($v = 0$) correlated to I*. Values of $f(N)$ are only calculated when the F_1 and F_2 components are resolved. Figure 15 shows a similar plot for CN correlated to I. The populations of each fine-structure component used to create these plots were corrected for the difference in LIF linestrengths,[46] which cause large inequalities at low N, but fall to less than a 10% correction [corresponding to $f(N)$ values of < 0.05] by $N = 10$. If we were to assume that the dissociation populated these levels simply as a function of their degeneracy, then it is trivial to show that, for all N,

$$f(N) = 1/(2N + 1). \tag{16}$$

This is plotted as the solid line in Figs. 14 and 15. We see that both channels exhibit deviations from this "statistical" limit. This behavior has been observed previously in other studies of the photodissociation of cyanogen halides.[30,31,35,41] For the I* channel, a net positive deviation in excess of the statistical limit for $20 \leqslant N \leqslant 35$ indicates that the F_1 channel is favored over F_2 in this region. Paul *et al.*[41] have previously observed a similar, net positive offset for $f(N)$ in the photodissociation of BrCN where they have established the $Br(^2P_{1/2})$ state as the only one populated.

The I channel, however, exhibits an oscillatory behavior as a function of N. Comparison with the results of Nadler *et al.* seems to indicate that the zeros of the function are shifted approximately five quanta to lower N for photolysis at 249 nm relative to 266 nm photolysis. Joswig *et al.*[35] found that the oscillations in $f(N)$ as a function of N at various photolysis wavelengths could be brought into coincidence by plotting $f(N)$ vs $N_{max} - N$, where N_{max} was the maximum allowed rotational level of the CN $(X, v = 2)$ fragment. This appears not to be the case for CN $(X, v = 0)$, where the maximum allowed values of N are 87 ± 2 for 249 nm and 78 ± 2 for 266 nm, and where the shift would in any case have to be to *lower N*.

E. Recoil velocity anisotropies

Figure 16 shows the effective system anisotropy parameters β_{eff} for the I* channel for CN ($v = 0$) as a function of

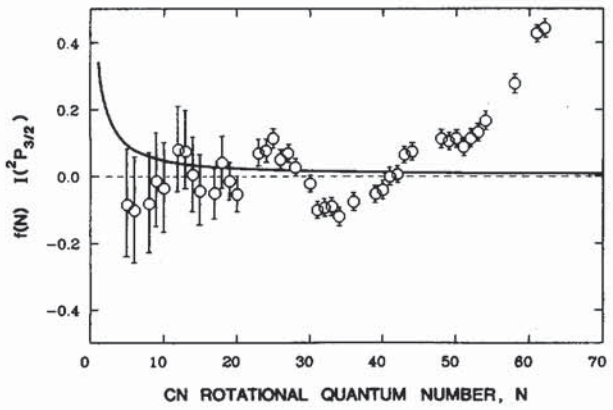

FIG. 15. The fine-structure difference function $f(N)$ vs N for photolysis yielding CN $(v = 0) + I(^2P_{3/2})$. Error bars (3σ) are obtained from those of the population analysis (Ref. 81). The solid line represents statistical behavior.

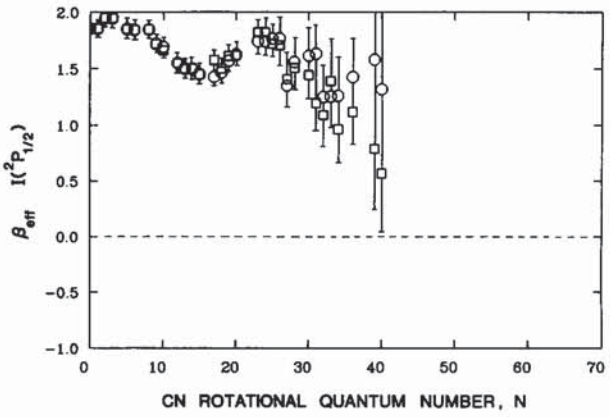

FIG. 16. The variation in β_{eff} vs N for photolysis yielding CN $(v = 0) + I(^2P_{1/2})$. The limits on the ordinate are the classical values. Within experimental error (3σ), the F_1 (squares) and F_2 (circles) components show identical behavior.

N. Analysis from experiments using a large number of laboratory geometries (see the Appendix) indicates that β_{eff} is very close to the true system anisotropy parameter β. In the current geometry, the correction to be made is in all cases less than 10% of the absolute values reported here. Apart from $N = 0$, where we can make some more detailed predictions, we discuss only *trends* in β_{eff} as a function of N and make no reference to absolute values. Our ability to isolate β_{eff} is somewhat correlated to the population of the particular CN $(v = 0, N) + (^2P_{1/2,3/2})$ half-collision pair under examination, hence the rather variable error bars.

For the I* channel, we see from Fig. 16 that β_{eff} starts close to the classical limit at low N ($\beta = 2$ for a parallel transition) and shows a general, but not monotonic, decrease to $\sim\beta_{eff} = 1.2$ around $N = 35$, where the fit is still reliable. Calculations suggest that, beyond $N = 10$, where hyperfine depolarization can be neglected,[83,84] the correction caused by $\mathbf{v} - \mathbf{J}$ vector correlations will *increase* β_{eff} (see the Appendix).

Measurement of the CN $(v = 0, N = 0)$ fragment is not complicated by vector correlations. The observed β_{eff} is therefore equal to the true system anisotropy parameter β and we can estimate the ICN dissociative lifetime.

We find the value of τ by solving Eq. (4) for γ, following Ref. 85, and using the value of I, the moment of inertia, from Cazzoli *et al.*[86] to evaluate Eq. (5). For $\beta = 1.85 \pm 0.05$, this yields

$$\tau \simeq 90 \pm 15 \text{ fs}.$$

We believe that this lifetime estimate is valid for decay of the ICN parent into the I* + CN $(v = 0, N = 0)$ fragments. However, the extraction of lifetime values from β_{eff} parameters is in general fraught with ambiguity caused by zero-point bending motion of the parent, which has not been properly incorporated into the model. However, for the production of CN $(v = 0, N = 0)$, we argue that bent configurations of the parent make a negligible contribution.

Figure 17 shows a plot of the β_{eff} values for the I channel for CN $(v = 0)$ as a function of N. This shows very interesting behavior, being negative at low N and becoming positive

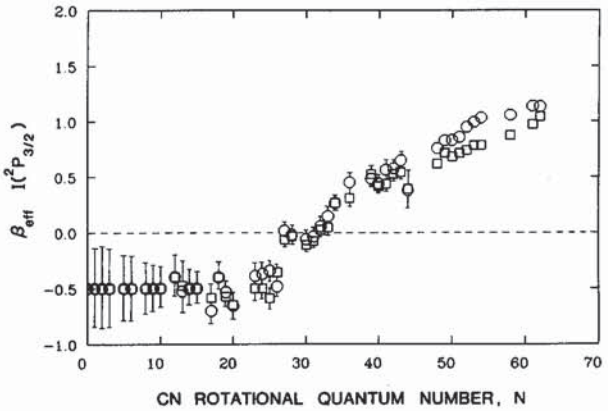

FIG. 17. The variation in β_{eff} vs N for photolysis yielding CN $(v=0)+\mathrm{I}(^2P_{3/2})$. The limits on the ordinate are the classical values. For $N>40$, the values for F_1 (squares) and F_2 (circles) are different. Error bars are 3σ and are smaller than the plotting symbol if not shown.

at high N. For this particular geometry, the change in sign of β_{eff} can *only* be explained by postulating a predominantly perpendicular transition giving rise to CN in low to medium N and a transition of predominantly parallel character giving rise to CN in medium to high N states, with gradual switching between the two. Even more remarkable might be the behavior of the F_1 and F_2 levels for the same value of N. Within experimental error (3σ), for high $N(\geqslant 40)$, the β_{eff} values for the F_1 and F_2 components are *different*, with β_{eff} (F_2) consistently higher than β_{eff} (F_1).

IV. DISCUSSION

By recording Doppler line shapes of the CN $(v=0,N)$ fragments produced in the 249 nm photodissociation of ICN, we have determined a number of scalar properties including the I*/I branching ratio, the F_1/F_2 population ratio, and the angular anisotropy of the recoiling fragments. The numerical values are presented in Table I. It is expedient to discuss the I* and I channels separately and then draw the threads together.

A. The I* channel

Outwardly, the dissociation dynamics producing this channel seem simple. A transition of essentially parallel character promotes photodissociation on a very repulsive, linear surface. The evidence for this comes from the large positive anisotropy parameters[19] ($\beta_{eff}=1.8$–1.9) observed for this channel (see Fig. 16), coupled with the correlation to predominantly low values of N.[16] At first sight the only unusual feature of this channel is the behavior of the fine-structure difference function $f(N)$ for $\sim 18\leqslant N\leqslant 35$ (see Fig. 14). We present tentative evidence that certain trajectories, asymptotically correlated to I*, sample a bent surface at some stage and, in doing so, experience torques yielding extra rotational excitation.

We note that in the region of interest, $18\leqslant N\leqslant 35$, the fine-structure difference function deviates from statistical. Joswig *et al.*[35] have already successfully interpreted such behavior for CN $(v=2)$ as a signature of nonadiabatic interactions causing transitions between potential energy surfaces. We suggest that the same behavior occurs here. A net positive offset for the $f(N)$ function was also observed in the work of Nadler *et al.*[31] (266 nm dissociation of ICN) and the work of Paul *et al.*[41] (dissociation of BrCN at various wavelengths) and seems to be a feature of the $^2P_{1/2}$ channel. It is not correct, however, to say that one particular spin–rotation doublet component is correlated to one particular halogen atom spin–orbit state; such a postulate is invalidated by the work of Joswig *et al.* and Nadler *et al.* It is quite probable that nonadiabatic forces also operate in the 266 nm dissociation of ICN and in the dissociation of BrCN in the $\tilde{A}$ continuum.

O'Halloran *et al.*[37] have studied the behavior of the alignment $A_0^{(2)}$ as a function of N (see Fig. 18). For low N the alignment reaches a maximum value of about -0.3 $(N=10)$, and as N increases, the alignment falls, tending toward about -0.1. At $N=38$, the limiting minimum is reached (at a value of -0.12). Between $N=10$ and $N=38$, the trend of decreasing $A_0^{(2)}$ is not smooth. Around $N=22,23$, the downward trend is interrupted, starting to rise again to a secondary maximum at $\sim N=28$ and then resuming its decline.

The range of N over which this deviation from monotonic behavior in the values of $A_0^{(2)}$ occurs matches almost exactly the range of N over which the $f(N)$ function deviates from statistical. We interpret the trend in the $A_0^{(2)}$ values (going from large and negative to zero) as the increasing importance of perpendicular character in the initial electronic transition. We will show that, *ceteris paribus*, this would normally cause a smooth transition in the alignment values. We therefore feel that the deviation from the expected monotonic behavior may be indicative of a secondary process, initially correlated to a parallel transition, contributing to extra population in the I* channel in this range of N.

If we examine the behavior of the effective system anisotropy parameter β_{eff} for this channel (Fig. 16), we see that, starting from $N=0$, the β_{eff} values initially fall smoothly, but at around $N=17,18$, the values rise to a secondary maximum around $N=25$ and then fall again. The analysis of the vector correlations in this geometry (see the Appendix) indicates that the overall correction to be made would be to increase the β_{eff} by not more than 10% of their absolute values. In addition, the correction to be made would be essentially constant and smooth over this range of N. It would certainly not give rise to the observed undulation in the β_{eff} values in Fig. 16. Again, the deviation from smooth behavior occurs in precisely the same range of N as the deviations in the $f(N)$ and $A_0^{(2)}$ functions. One possible explanation of the overall decrease in β_{eff} for increasing N is to hypothesize the contribution of a perpendicular transition.

We recognize that molecules initially prepared via a perpendicular transition (to surfaces correlated asymptotically with I) could cross onto surfaces correlated with I* via seams of interaction.[87] The β_{eff} values reflect only the initial transition symmetry in the limit of rapid dissociation and would consequently be a superposition of parallel and perpendicular transitions. Intuitively, we would expect the con-

TABLE I. Compilation of the relative population $\Phi_{1*}(N)$, fine-structure difference functions, and effective system anisotropy parameters for the CN ($v=0,N$) levels studies in the present work. The error (3σ) on $\Phi_{1*}(N)$ is nowhere greater than 0.07. The errors on the $f(N)$ and β_{eff} values vary with N and may be judged from Figs. 14–17. The functions $f(N)$ have only been calculated for lines where spectroscopic resolution was achieved. Values for $N<15$ are from interactive simulations.

N	Relative Population	$\Phi_{1*}(N)$	$f_1(N)$	$f_{1*}(N)$	$\beta_{\text{eff}}(I,F_1)$	$\beta_{\text{eff}}(I,F_2)$	$\beta_{\text{eff}}(I^*,F_1)$[a]	$\beta_{\text{eff}}(I^*/F_2)$[a]
0	0.16	0.92			−0.50	−0.50	1.85	1.85
1	0.43	0.92			−0.50	−0.50	1.85	1.85
2	0.51	0.90			−0.50	−0.50	1.94	1.94
3	0.69	0.90			−0.50	−0.50	1.94	1.94
5	0.53	0.89	−0.08	0.06	−0.50	−0.50	1.85	1.85
6	0.54	0.87	−0.10	0.05	−0.50	−0.50	1.84	1.84
8	0.65	0.81	−0.08	0.06	−0.50	−0.50	1.84	1.84
9	0.67	0.80	−0.01	0.04	−0.50	−0.50	1.72	1.72
10	0.83	0.77	−0.03	0.02	−0.50	−0.50	1.66	1.69
12	0.69	0.77	0.07	0.03	−0.39	−0.39	1.54	1.54
13	0.85	0.72	0.07	0.02	−0.47	−0.52	1.50	1.50
14	0.74	0.65	0.00	0.03	−0.50	−0.50	1.50	1.50
15	0.77	0.67	−0.04	0.04	−0.50	−0.50	1.45	1.45
17	0.73	0.71	−0.05	0.04	−0.58	−0.70	1.57	1.42
18	0.78	0.68	0.04	0.06	−0.40	−0.40	1.50	1.46
19	1.00	0.66	−0.01	0.04	−0.57	−0.53	1.61	1.57
20	0.94	0.62	−0.05	0.10	−0.64	−0.65	1.61	1.62
23	0.86	0.55	0.06	0.15	−0.50	−0.38	1.82	1.74
24	0.93	0.51	0.07	0.13	−0.50	−0.37	1.82	1.74
25	0.88	0.48	0.11	0.12	−0.58	−0.34	1.72	1.76
26	0.87	0.47	0.05	0.17	−0.35	−0.48	1.70	1.76
27	0.89	0.54	0.06	0.17	−0.06	0.01	1.40	1.35
28	0.90	0.49	0.02	0.18	−0.03	−0.02	1.50	1.56
30	0.73	0.40	−0.02	0.13	−0.11	−0.06	1.44	1.61
31	0.72	0.37	−0.10	0.20	−0.07	−0.03	1.19	1.63
32	0.73	0.36	−0.09	0.12	0.02	0.05	1.09	1.25
33	0.67	0.29	−0.09	0.05	0.04	0.14	1.39	1.25
34	0.70	0.27	−0.12	0.10	0.26	0.26	0.96	1.26
36	0.65	0.17	−0.07	0.00	0.30	0.44	1.11	1.42
39	0.59	0.09	−0.05	0.05	0.52	0.48	0.78	1.58
40	0.69	0.09	−0.04	0.08	0.41	0.43	0.56	1.31
41	0.69	0.10	−0.00	−0.82	0.43	0.56	1.50	1.50
42	0.67	0.02	0.00	−0.21	0.52	0.57	1.50	1.50
43	0.66	0.01	0.06	1.00	0.54	0.64	1.50	0.00
44	0.68	0.00	0.07		0.38	0.37		
48	0.66	0.00	0.11		0.61	0.75		
49	0.63	0.00	0.10		0.71	0.82		
50	0.67	0.00	0.11		0.68	0.83		
51	0.65	0.00	0.08		0.71	0.85		
52	0.58	0.00	0.11		0.73	0.94		
53	0.51	0.00	0.13		0.78	0.99		
54	0.51	0.00	0.16		0.78	1.03		
58	0.27	0.00	0.27		0.87	1.05		
61	0.14	0.00	0.42		0.97	1.13		
62	0.09	0.00	0.44		1.04	1.13		

[a]A combination of spectroscopy and very low population rendered the final three measurements in these columns difficult. Fixed values ($\beta_{\text{eff}}=1.50$) were used for population assessment, but have not been included in Fig. 16. For $N=43$, there was no detectable population in the F_2 component. Consequently, $f(43)=1.00$ (with large error) and $\beta_{\text{eff}}(I^*,F_2)=0.00$ for convenience. Again, these have not been included in the relevant plots.

tribution from the bent, perpendicular surface to be lower for CN in low N and to rise as the CN is formed in increasingly higher N, giving a general decrease in β_{eff} from the limiting parallel values observed at low N. The same argument also explains the overall trend in the $A_0^{(2)}$ values of O'Halloran *et al.*,[37] shown in Fig. 18. A parallel transition would yield negative values of $A_0^{(2)}$, while a perpendicular transition would give positive values. From our study it would appear that CN ($v=0$) in low N are coming from a predominantly parallel-type dissociation and we see large negative $A_0^{(2)}$ parameters as expected. We note that the β_{eff} values approach more closely the limiting classical values for a parallel transition than do the $A_0^{(2)}$ values. From the above arguments we suspect the increasing involvement of perpendicular transitions yielding CN ($v=0$) in medium and high N. This is reflected in the overall trend of $A_0^{(2)}$ becoming less negative. Further support for the mixed character of the transition is provided by examining the $\mathbf{v}-\mathbf{J}$ vector correlation (see the Appendix).

A theoretical treatment of the dynamics of ICN photodissociation at a number of wavelengths by Goldfield *et al.*[15] (including 249 nm) has yielded two empirical repulsive surfaces correlated to the two iodine spin–orbit channels. In the linear configuration, these surfaces are seen to cross and re-

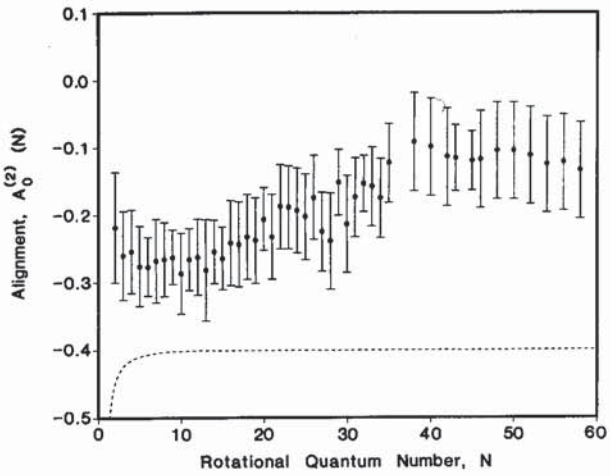

FIG. 18. Alignment $A_0^{(2)}$ as a function of N for CN $X\,^2\Sigma^+$ $v=0$ reproduced from Ref. 37. Values have been corrected for experimental geometry, spin depolarization, and velocity correlations. Error bars represent statistical uncertainties and estimates for systematic uncertainty. The dashed curve shows the limiting values for a pure parallel transition.

cross [see Fig. 3(a) of Ref. 15]. These surfaces were constructed to reproduce the quantum yields and rotational envelopes at dissociation wavelengths of 266 nm and longer, but give poor results for shorter wavelength dissociation. Goldfield *et al.* postulated the involvement of a third surface, perpendicular and bent in nature, to explain the shorter wavelength results. As we shall see, this hypothesis is probably correct, but here we concentrate on trajectories to I*. Goldfield *et al.* noted that trajectories leading to CN in intermediate N did indeed sample portions of the bent surface before recrossing to the linear surface and subsequently evolving, correlating asymptotically to the I* state. The crossing and recrossing shown in the figure for linear ICN is somewhat misleading, as it was assumed that the coupling matrix elements were zero at $\theta = 0°$ because the surface correlating to I is not of 0^+ symmetry at $\theta = 0°$. Despite these shortcomings, we use these potential energy surfaces to provide an approximate picture of the photodissociation dynamics.

From the above arguments we conclude that the dissociation to I* is not merely a collinear dissociation on surfaces of parallel character, but represents, in addition, contributions from crossing and recrossing to one or more bent surfaces.

B. The I channel

The contribution of the I channel rises monotonically from 4% ($N=0$) to 100% ($N>40$) [see Fig. 13(a)]. The fine-structure difference function $f(N)$ shows oscillations as a function of N (see Fig. 15), which are now a familiar feature of these systems.[30,31,35,41] As previously stated, there seems to be no simple angular momentum scaling between the present results and those for photolysis at 266 nm. Such scaling was observed for the CN ($v=2$) fragments from dissociation at 249, 266, and 281.5 nm.[35]

The most striking feature of the I channel is the variation of β_{eff} with N (see Fig. 17). There is a smooth transition from negative values at low N to positive values at high N. To explain this behavior, we must postulate the additional involvement of a perpendicular-type transition to a surface (surfaces) correlated asymptotically to I. We can further state that this third surface is the dominant pathway for production of CN ($v=0$) + I($^2P_{3/2}$). Evidence for this comes from the present work and the following observations from previous studies of this system:

(i) We note that the I* quantum yield at 249 nm obtained by Hess and Leone[36] and by us is lower than that for photolysis at 266 nm (44% vs 65%).[31] Suppose that we invoke the predictions of the Landau–Zener curve-crossing mechanism[88] in a two-surface model. We would expect that as the energy available for translation (product separation) is decreased, the efficacy of curve crossing would increase and Φ_{I^*} would concomitantly decrease. This behavior was noted by Goldfield *et al.*[15] in their theoretical study of this system. The involvement of a third surface asymptotically connected to I($^2P_{3/2}$) is necessary to explain the quantum yield observations.

(ii) We note that measurements of the quadrupole moment of the angular momentum distribution,[32,37] the $A_0^{(2)}$ alignment parameter, show large fluctuations as a function of N (see Fig. 18). The observations are that, at low N, where the I* channel predominates, the alignment values are large and negative, reflecting the rapid, parallel nature of the dissociation leading to I*. As N increases, the values of $A_0^{(2)}$ become progressively smaller, reaching limiting values of ~ -0.1 at $N \simeq 40$. The work of O'Halloran *et al.*[37] included measurements of alignment at higher N, whereupon the $A_0^{(2)}$ value was observed to become more negative again, reaching a value of ~ -0.15 at $N=58$. The alignment measurements are probing the fundamental underlying vibronic nature of the transitions involved in photodissociating at this wavelength. O'Halloran *et al.* postulated the influence of nonadiabatic forces to explain the change in alignment as a function of N, but, with the benefit of the present results, we suggest that this is not the principal reason for the observed fluctuations.

A better explanation is that the trend of decreasing $A_0^{(2)}$ as N increases results from an admixture of CN originating from both parallel and perpendicular character surfaces,[15] with the increasing importance of the perpendicular I channel with increasing N. The observation that the β_{eff} values *do* become large and positive for high N for the I channel indicates that some CN are being produced from a transition of parallel character. This cannot be a direct excitation and is most likely to be the glancing intersection of a surface asymptotically correlated to I* (initially accessed in the absorption step) and a bent surface, asymptotically correlated to I. This intersection would appear to be the major source of CN ($v=0,N$) + I($^2P_{3/2}$) for very high N. The effect of the switch can be seen in the trend of the alignment values (see Fig. 18), where for $N>40$ we observe a progression towards increasingly negative values. The increasing negative values reflect the growing importance of the initial parallel nature of the production of CN in these N levels. These observations immediately allow us to state that the passage through the glancing intersection between two surfaces generates larger

intramolecular torques than does the "embedded" nature of torques caused by the immediate Franck–Condon promotion to a bent state. We can reconcile the above observations by noting that direct promotion to a bent state [correlated to $I(^2P_{3/2})$] will deposit the $t=0$ wave packet in a region of the bent surface where $\delta V/\delta\theta$ is small or zero. The dynamics governing the development of torque are essentially those of relaxation from the bent geometry to the (necessarily) linear geometry in the asymptote. (We note that at 300 K about 30% of ICN molecules in the ground electronic state have one quantum of vibrational excitation in the bending mode. Intuitively we would expect superior Franck–Condon overlap between this vibrationally excited level and the bent electronically excited state. We suggest that the quantum yield Φ_{I^*} might increase in the photolysis of a jet-cooled sample of the parent.)

In contrast, the act of passage through the glancing intersection will expose the molecule to very large gradients of the potential with respect to θ, i.e., large $\delta V/\delta\theta$. This is particularly apparent in Fig. 4 of Goldfield *et al.* (adapted as Fig. 19 here), where the potential changes by 8–10 000 cm^{-1} over a very small range of θ between the minima of the surfaces for small extensions of R(I–CN). Our data are not sufficiently structured, however, to allow us to make a realistic deconvolution to separate the contributions of the two channels. Again we should note that the coupling terms used by Goldfield *et al.* dictate zero interaction at $\theta=0°$, with the interaction increasing quadratically in $\sin\theta$; however the figures serve to illustrate the point under discussion.

(iii) We note that the I*/I ratio becomes unity at $N=26$, where (interpolating a smooth trend in β_{eff}) the β_{eff} values are still comfortably negative. By the time the I channel is completely dominant ($N\geqslant 40$), the β_{eff} values are still a long way from the parallel limit, even allowing for the influence of vector correlations. (The β_{eff} values seem to be rising at the point at which our study stops but here the populations are negligible.)

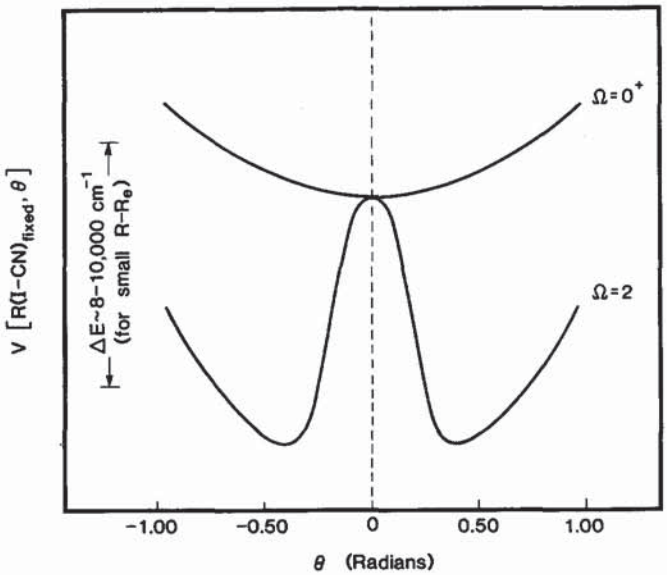

FIG. 19. Cut through the schematic potential intersection of the $\Omega=0^+$ and $\Omega=2$ surface (adapted from Ref. 15) showing the large potential gradient $\delta V/\delta\theta$ in the region of R(I–CN) close to the Franck–Condon region.

At the moment we are at a loss to explain two of the more subtle features of our experimental observations. Firstly, in Fig. 17 we see that for $N>45$ the β_{eff} parameters for the F_1 and F_2 components are different within experimental error. This is remarkable as, even at $N=75$, the F_1, F_2 levels are only separated by 0.5 cm^{-1} in the asymptote, yet the F_2 component shows a significantly and consistently higher β_{eff} value than the F_1 component. This difference in β_{eff} is also obvious in Fig. 2 (final panel) of Nadler *et al.*,[31] where for $N=57$ the F_2 component shows a larger β_{eff} value (although these authors did not comment on this).

Secondly, we note (from Fig. 15) that in the same region where the β_{eff} values show significant differences for the F_1/F_2 components, the fine-structure difference function $f(N)$ stops oscillating and assumes large positive values. Our detection sensitivity did not allow us to probe past $N=62$ with any great reliability, but in future experiments it should be possible to examine the trend in $f(N)$ to higher N.

Both of these features must be highly quantum mechanical in origin, probably linked to the coupling of the electronic and rotational degrees of freedom in the dissociating molecule, as already discussed by Joswig *et al.*[35] Band, Freed, and Singer have been engaged in a thorough theoretical treatment of the subtleties of diatomic photodissociation for some considerable time.[89] They have based the work on the precept "that the Born–Oppenheimer approximation must *always* fail upon dissociation to fragments with nonvanishing electronic angular momentum."[90] The resulting nonadiabatic interactions come to prominence in the so-called molecular recoupling region, found at intermediate internuclear distance between the molecular and fragment limits. Among the predictions of the theory are the nonstatistical populations of the atomic fine-structure states (varying as a function of photolysis energy) and the intriguing observation that the fine-structure states themselves may have different angular distributions and polarized angular momentum distributions. It is reasonable to suppose that the precept can be extended to triatomic photodissociation, but the theoretical followup would be formidable.[91] We observe here two of the predicted effects and we have observed fine-structure-dependent polarization anisotropy in independent experiments.[92,93]

C. General discussion

It is clear that any discussion of the photodissociation dynamics of ICN in the $\tilde{A}$ continuum must be couched in terms of (at least) a three-surface model. The electronic structure of the $\tilde{A}$ continuum is currently the subject of debate: there are arguments for both $\pi^3\pi^*$ and $\pi^3\sigma^*$ electronic configurations.[20,94] For comparison, we refer to the analogous CH_3I $\tilde{A}$-continuum manifold, which is in some ways better understood.[72,73,75,76,78,95–99]

Initial absorption in ICN at 249 nm is by states of $\Omega=0$ character, giving parallel transitions, and $\Omega=1$ states, yielding perpendicular transitions. Vigué *et al.*[17] hypothesize that these are the $^3\Pi_{0+}$ and $^1\Pi_1$ states of the $\pi^3\sigma^*$ configuration. These can be likened to the $^3Q_0$ and $^1Q_1$ states already identified in CH_3I.[72,73,75,76,78,95–99] The $\pi^3\sigma^*$ configuration also generates states of $^3\Pi_1$ and $^3\Pi_2$ character. The

$^3\Pi_{0+}$ state correlates asymptotically with I* and the majority of I* production is associated with direct evolution on this surface. We interpret the *overall* trends in the β_{eff} values and $A_0^{(2)}$ values at 249 nm as the growing contribution from a perpendicular electronic transition with subsequent curve crossing as the CN is formed in increasingly higher N in this channel.

The I* channel also shows effects from crossing and recrossing, evidenced by the discontinuities in the $\beta_{\text{eff}}, f(N)$, and $A_0^{(2)}$ plots. We believe that the origins of these lie in nonadiabatic transitions of the type discussed by Joswig *et al.*,[35] O'Halloran *et al.*,[37] and Vigué *et al.*,[17] involving interactions with surfaces of $\Omega = 1$ character.

The I channel shows contributions from initial electronic transitions of both perpendicular and parallel character. Goldfield *et al.*[15] have identified one interaction as the glancing intersection of the $^3\Pi_{0+}$ state with a state of $\Omega = 2$ character (perhaps $^3\Pi_2$ from the $\pi^3\sigma^*$ configuration), optically disconnected and correlated asymptotically with the I channel. We believe this interaction to be the source of $I(^2P_{3/2}) + CN\ (v = 0)$ fragments where the CN is found in very high rotational levels. The positive β_{eff} parameters found for these fragments reflect the parallel-type transition responsible for their origin, while the high rotational angular momentum is a signature of the large $\delta V/\delta\theta$ term involved in curve crossing. The perpendicular component of the I channel seen to correlate with low N is probably a direct promotion, i.e., optically connected to the ground state. Given the energy ordering of the states, this is most likely to be the $^1\Pi_1$ state (perhaps from the $\pi^3\sigma^*$ configuration), as discussed by Vigué *et al.*

Our overall picture is summed up in Fig. 20. This is a schematic representation of potentials consistent with our arguments, shown at $\theta = 0°$ (linear geometry). We make no comment as to which electronic configuration could generate these potentials; the electronic nature of the continuum remains to be established.

The further eludication of the photodissociation dynamics of ICN in the $\tilde{A}$ continuum would be greatly aided by the calculation of *ab initio* surfaces for the ground and valence excited states. Recent results from calculations on the analogous CH_3I manifold[98,99] indicate that quantum chemistry can now generate realistic potentials for systems with large spin–orbit interactions (i.e., those containing I atoms). Morokuma and co-workers have extended their study to the calculation of nonadiabatic coupling terms, another vital and profitable extension of the current theory.[98] We hope that similar calculations for ICN will be forthcoming. The behavior of the surfaces and their coupling with respect to the bending angle would be of particular interest.

Hasselbrink *et al.*[39] have photodissociated ICN at 249 nm using circularly polarized photolysis light. Probing the CN ($v = 0$) fragments, again with circularly polarized light, they observed strong orientation of the CN fragment. We reproduce their results as Fig. 21, where we have plotted the value of the $A_0^{(1)}$ moment as a function of N. Hasselbrink *et al.* hypothesized that the sign of the orientation was linked to the spin–orbit state of the iodine atom in some way and, referring to Figs. 12 and 13(a), we see that the trend in $A_0^{(1)}$ vs N is very reminiscent of the switching between the two exit channels. The plots of $A_0^{(1)}$ and I*/I exit-channel switching as a function of N do not quite superimpose. The magnitude of orientation seems to be greater for CN ($v = 0$) correlated to the I channel than for the I* channel. This is probably linked to the effects of amplification of angular momentum as discussed by Vigué *et al.*[17] for ICN and lately by Dixon[100] for NH_3.

Finally, we note that the "lifetime" estimate that we

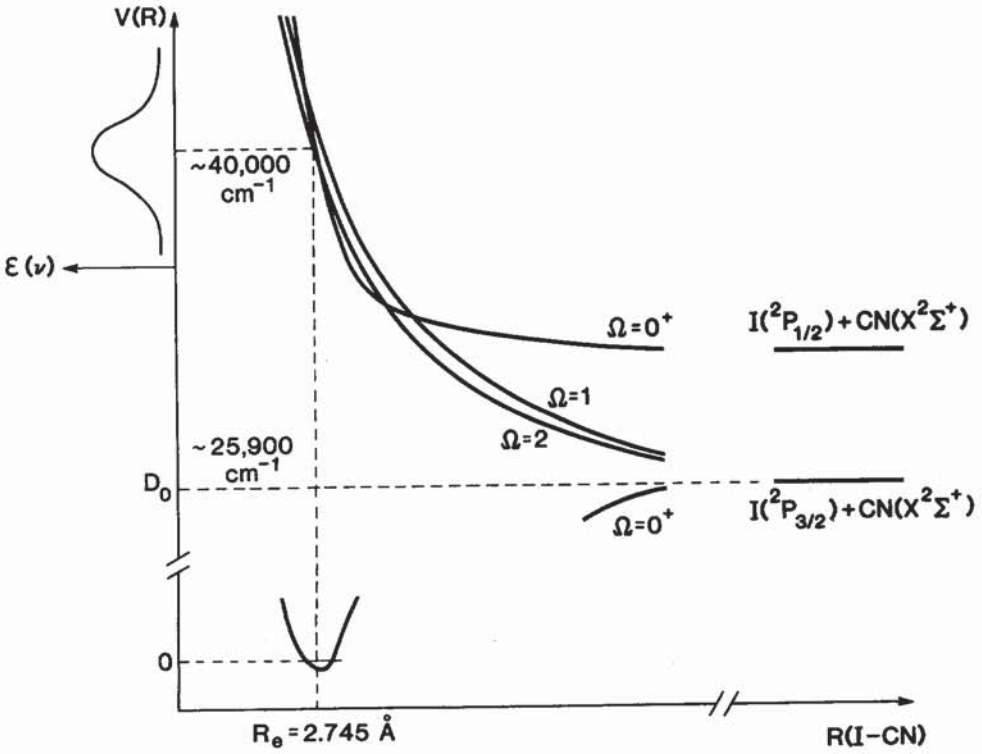

FIG. 20. Cut through hypothetical potential energy surfaces for ICN at $\theta = 0°$ showing three interacting excited state surfaces in the Franck–Condon region.

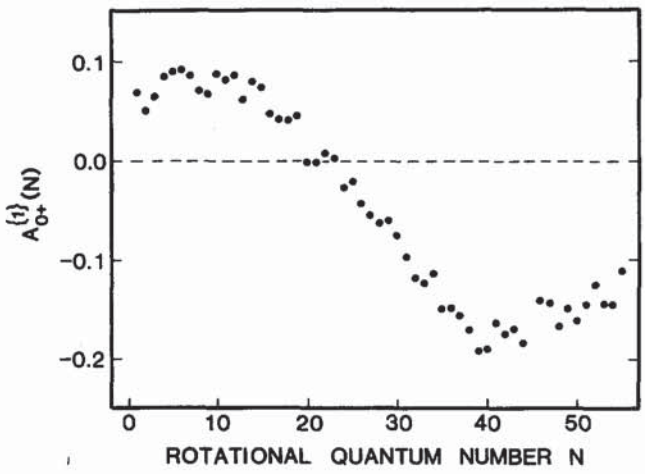

FIG. 21. The dipole moment $A_0^{(1)}$ (the orientation) vs N for CN ($v=0$) from the photolysis of ICN at 249 nm (reproduced from Ref. 39).

obtain here (<100 fs) is more rapid than that obtained by Dantus *et al.*,[40] who observed $\tau\sim200$ fs at 306 nm and $\tau\sim160$ fs at 285 nm. One may argue about the validity of comparison of the two methods; however, the observed general decrease in lifetime with increasing photolysis energy is known from a number of other systems, CH_3I[78] and H_2O_2[101–103] being two examples. The reasonable agreement and rational trend of the measurements give us confidence in our earlier treatment of $\beta_{\rm eff}$ in that the dissociation is *very* rapid on the time scale of molecular rotation and that, consequently, little rotational smearing mars the results.

V. CONCLUSION

We have used Doppler spectroscopy to elucidate the scalar and some vector properties of the dissociation of ICN at 249 nm. We have demonstrated that at this wavelength the description of the dissociation dynamics must be posed in terms of a three-surface model. Evidence has been presented for nonadiabatic processes affecting both the dissociation to $I(^2P_{1/2})$ and $I(^2P_{3/2})$. A model involving multiple surface interactions has been presented. This model not only accounts for the observations in this work, but also explains certain facets of previous experimental data.

APPENDIX: VECTOR CORRELATION ANALYSIS

In the course of formulating a plausible explanation for the N-dependent, nonstatistical populations of the F_1/F_2 components, Joswig *et al.*[35] developed a model Hamiltonian for the system incorporating a term

$$\mathbf{N}\cdot\mathbf{J}_{12}/2\mu R^2,$$

where $\mathbf{J}_{12}$ is the resultant of the iodine atom electronic momentum and the CN electron spin angular momentum. This constitutes (in the derivative formulation) a force directed *out of the plane of scattering* defined by the three atoms.

Classically, forces act in a pairwise additive fashion between the atoms and it would be expected that all forces act "in plane." The logical extension of this postulate is that, in the asymptote, the vectors representing the velocity of the CN fragment $\mathbf{v}$ and the rotational angular momentum $\mathbf{J}$ will be *perpendicular*. This has been the tacit assumption in a number of studies of the photodissociation of triatomic molecules.[101,104–106]

We hypothesize, however, that the existence of the relativistic force described by Joswig *et al.*[35] will give rise to a nontrivial projection of $\mathbf{v}$ on $\mathbf{J}$ (i.e., no longer an expectation value of 90° for $\cos^{-1}(\mathbf{v}\cdot\mathbf{J})$). The obvious way to test this hypothesis might appear to be a full sub-Doppler polarization analysis of the LIF transitions of the CN fragment in the manner advocated by Dixon[52] and Houston and coworkers.[54,55] In particular, a nontrivial value of the bipolar harmonic describing the $\mathbf{v}\cdot\mathbf{J}$ correlation in the formalism of Dixon might well be proof of the existence of an out-of-plane force.

We have performed this analysis for $N=0,12,24,33,49$, and 58, spanning almost the full range of detectable CN ($v=0,N$) quantum states. First, we justify our previous statements that in the chosen geometry the correction to be made to $\beta_{\rm eff}$ to yield "$\beta_{\rm true}$" is not more than 10% of the value of $\beta_{\rm eff}$. From Dixon,[52] we have

$$I(\nu)\propto\frac{c}{2\nu_0|\mathbf{v}|}\left\{g_0+g_2P_2\left[\frac{c(\nu-\nu_0)}{\nu_0|\mathbf{v}|}\right]\right\}, \tag{A1}$$

where

$$g_0=b_0+b_1\beta_0^2(02) \tag{A2}$$

and

$$g_2=b_2\beta_0^2(20)+b_3\beta_0^0(22)+b_4\beta_0^2(22). \tag{A3}$$

In this formulation, g_2 contains factors dependent on the excitation–detection geometry.

Here, the $\beta_0^K(k_1k_2)$ are renormalized bipolar moments. These are the expectation values of the bipolar harmonic functions describing the expansion of the system in $\boldsymbol{\mu},\mathbf{v},\mathbf{J}$, space. Equation (A1) is itself an approximation as it neglects higher order terms in the expansion of the system in the spherical harmonic basis. It is known,[52] however, that the multipliers of the higher order terms are approximately one order of magnitude smaller than those of terms considered in Eq. (A1). At our current level of approximation, we may safely neglect higher order terms. Two of the renormalized bipolar moments, $\beta_0^2(20)$ and $\beta_0^2(02)$, are related to the more common photofragment angular distributions anisotropy and photofragment alignment parameters by

$$\beta_0^2(20)\simeq\tfrac{1}{2}\beta_{\rm true} \tag{A4a}$$

and

$$\beta_0^2(02)\simeq\tfrac{5}{4}A_0^{(2)}. \tag{A4b}$$

The other two, $\beta_0^0(22)$ and $\beta_0^2(22)$, represent "newer" quantities, where $\beta_0^0(22)$ describes the $\mathbf{v}$–$\mathbf{J}$ correlation and $\beta_0^2(22)$ provides a measure of the ($\mathbf{v}$–$\mathbf{J}$–$\boldsymbol{\mu}$) correlation (the "triple vector" correlation). The b_0–b_4 parameters are simply numbers; multipliers that depend on the system geometry and angular momentum considerations as discussed by Greene and Zare.[107]

We rearrange Eq. (A1) slightly to yield a more familiar form, viz.,

$$I(\nu) \propto \frac{g_0 c}{2\nu_0|\mathbf{v}|}\left\{1+\beta_{eff}P_2\left[\frac{(\nu-\nu_0)c}{\nu_0|\mathbf{v}|}\right]\right\}, \tag{A5}$$

where

$$\beta_{\text{eff}} = \frac{b_2\beta_0^2(20)+b_3\beta_0^0(22)+b_4\beta_0^2(22)}{b_0+b_1\beta_0^2(02)}. \tag{A6}$$

For $R(58)$, calculations for the b_1 multipliers yield[57]

$$\left.\begin{aligned} b_0 &= 0.8974 \\ b_1 &= 0.1235 \\ b_2 &= 1.7948 \\ b_3 &= 0.3088 \\ b_4 &= -0.1765 \end{aligned}\right\}. \tag{A7}$$

If, for the moment, we assume that the dissociation originates from a parallel-type transition and takes place promptly (axial recoil approximation), we obtain (from Dixon,[52] Fig. 3, case b) the limiting values for the $\beta_0^K(k_1k_2)$ parameters

$$\left.\begin{aligned} \beta_0^2(20) &= 1 \\ \beta_0^0(22) &= -0.5 \\ \beta_0^2(22) &= +0.5 \\ \beta_0^2(02) &= -0.5 \end{aligned}\right\}. \tag{A8}$$

This analysis assumes $\mathbf{v}\|z$, $\mathbf{J}\perp z$, and $\mathbf{v}\perp\mathbf{J}$. Substituting Eqs. (A7) and (A8) into Eq. (A6), we obtain

$$\beta_{\text{eff}} = 1.8574. \tag{A9}$$

This should be compared to the predicted value of $\beta_{\text{true}} = 2$. Hence, β_{eff} differs from β_{true} by approximately 10%. This result does not change significantly for values of N ranging from 10–60. If we assume a perpendicular-type transition (yielding Dixon's cases c and e in Fig. 3 of Ref. 52), then the magnitude of the correction to β_{eff} is still less than 10% of the absolute value. However, for this transition symmetry the value of β_{eff} exceeds the magnitude of β_{true}.

Secondly, preliminary analysis[57] has yielded estimates for the expectation value of the angle between v and J, taking the results of the fit of Doppler profiles to Eq. (A5) at face value. For $N=49$ and $N=58$, we obtain for each fine-structure component the values listed in Table II. We offer two comments on these results.

(a) The disquieting scatter between the results for two fine-structure components for one N merely reflects the general unsuitability of the CN $B\,^2\Sigma^+ - X\,^2\Sigma^+$ transition as a vehicle for studying vector correlations in CN reaction products. The greatest variation of the multipliers of the bipolar harmonics, the b_i coefficients, occurs for Q branches[52] and the $\beta_0^K(k_1k_2)$ values will consequently be better determined for systems where the analysis can include Q-branch transitions along with P- and R-branch transitions. In the present system, we can only analyze P and R transitions. Small differences in parameter space are magnified by the inversion procedure. This is not to say, however, that we expect the values for the fine-structure components to be identical.[89] With hindsight, it may be that the $A\,^2\Pi - X\,^2\Sigma^+$ transition is more suitable for probing the influence of vector correlations in CN reaction products as this system offers the bonus of Q-branch transitions.

TABLE II. Values of the angle between v and J, as extracted from an analysis of Doppler profiles taken under various experimental geometries, for $N=49$ and $N=58$ in the CN $(X,v=0)$ manifold. Errors represent one standard deviation.

N	J	θ_{vJ} (degrees)
49	48.5 (F_2)	71 ± 6
49	49.5 (F_1)	78 ± 6
58	57.5 (F_2)	67 ± 7
58	58.5 (F_1)	80 ± 6

(b) These results, particularly those for the F_2 components, are obviously nonphysical. We refer to the usual angular momentum balance

$$\mathbf{J}_{\text{ICN}} + \mathbf{J}_{\text{photon}} = \mathbf{J}_{\text{CN}} + \mathbf{J}_1 + \mathbf{l}, \tag{A10}$$

where l is the orbital angular momentum of the recoiling photofragments.

We may distinguish several limiting cases. If the parent rotation can be neglected, then $\mathbf{J}_{\text{CN}} = -\mu\mathbf{v}\times\mathbf{b}$ and $\mathbf{J}_{\text{CN}}$ must lie perpendicular to v and b, i.e., to the ICN scattering plane. For this limiting case, the angle between v and J is strictly 90° (neglecting the few units of angular momentum provided by the dipole photon and the fine structure of the I atom).

However, under thermal conditions, the most probable value of $\mathbf{J}_{\text{ICN}}$ is about 30. A limiting case that more closely approximates the present experiment is to consider $\mathbf{J}_{\text{ICN}}$ to be large and to lie perpendicular to the ICN internuclear axis (linear molecule). Then, if the photodissociation is prompt on the time scale of parent rotation, once again v and $\mathbf{J}_{\text{CN}}$ are perpendicular within the approximation of Eq. (A11). Our estimate of ICN photodissociation lifetimes implies that the ICN parent rotates only a few degrees.

It might be wondered how these arguments would be modified by excitation of the ICN bending mode (or by zero-point bending motion). For this case, it is possible for $\mathbf{J}_{\text{ICN}}$ to have a nonnegligible component in the ICN scattering plane, but its magnitude is not sufficient to account for the angle between v and $\mathbf{J}_{\text{CN}}$ implied by the analysis in Table II.

We also note that the $\mathbf{N}\cdot\mathbf{J}_{12}/2\mu R^2$ term in the Hamiltonian constitutes a very subtle effect. Its ability to influence dramatically the dissociation dynamics stems not from its size, but the ability to introduce nonadiabatic coupling at seams of curve crossings.[35] It is also not realistic that this force could tip the plane of rotation of the CN fragments by up to 20° relative to the initial plane of scattering.

Consequently, we are forced to consider another explanation for the observations. In the main paper, we have presented substantial evidence for the influence of a mixed perpendicular/parallel transition in the initial photon absorption step. This perturbation of the reference frame around which the vector correlation theories are built[52,54,55] is sufficient to impair severely our ability to isolate nontrivial values of the correlation moments. We note the previous work of Sivakumar *et al.*,[108] who photodissociated OCS at a variety of wavelengths. They observed radical variations in the β_{eff} values as a function of N, similar in some ways to

those we observe here. Sivakumar *et al.* were able to analyze quite successfully the Doppler profile set in terms of a linear combination of parallel and perpendicular components in the initial photon absorption step. They assumed that the bipolar harmonics describing the system[52] were at their physical limits for each component and, using linear combination, were able to extract the relative contributions of parallel and perpendicular electronic character as a function of N. Our data (Table II) are clearly inconsistent with dissociation on a single surface and we suggest that these data are a further manifestation of the mixed electronic character of the dissociation dynamics.

ACKNOWLEDGMENTS

We are grateful to Maureen O'Halloran, David Rakestraw, and Patrick Vaccaro for numerous useful suggestions concerning the experimental procedure, and to Ivan Powis (Nottingham University) for advice concerning the use of NAG routines. We also thank Eckart Hasselbrink for a legacy of excellent software and lab notes and the authors of Refs. 5, 19, 97, and 100 for providing preprints of their work. JFB thanks SERC (UK) for support under the SERC/NATO postdoctoral fellowship scheme. This work has been supported under NSF-PHY-88-05603.

[1] S. R. Leone, Acc. Chem. Res. **16**, 88 (1983).
[2] R. Bersohn, J. Phys. Chem. **88**, 5145 (1984).
[3] J. P. Simons, J. Phys. Chem. **91**, 5378 (1987).
[4] P. L. Houston, J. Phys. Chem. **91**, 5388 (1987).
[5] G. E. Hall and P. L. Houston, Annu. Rev. Phys. Chem. **40**, 375 (1989).
[6] Faraday Discuss. Chem. Soc. **82**, (1986); special issue.
[7] Y. B. Band and K. F. Freed, J. Chem. Phys. **63**, 3382 (1975).
[8] M. D. Morse, K. F. Freed, and Y. B. Band, J. Chem. Phys. **70**, 3604 (1979).
[9] M. D. Morse, K. F. Freed, and Y. B. Band, J. Chem. Phys. **70**, 3620 (1979).
[10] M. D. Morse and K. F. Freed, J. Chem Phys. **74**, 4395 (1981).
[11] J. A. Beswick and W. M. Gelbart, J. Phys. Chem. **84**, 3148 (1980).
[12] M. D. Pattengill, Chem. Phys. **78**, 229 (1983).
[13] M. D. Pattengill, Chem. Phys. **87**, 419 (1984).
[14] R. Schinke and V. Engel, J. Chem. Phys. **83**, 5068 (1985).
[15] E. M. Goldfield, P. L. Houston, and G. S. Ezra, J. Chem. Phys. **84**, 3120 (1986); Note added in proof; see also H. Guo and G. C. Schatz, J. Chem. Phys. **92**, 1634 (1990).
[16] C. H. Dugan and D. Anthony, J. Phys. Chem. **91**, 3929 (1987).
[17] J. Vigué, B. Girard, G. Gouédard, and N. Billy, Phys. Rev. Lett. **62**, 1358 (1989).
[18] R. Heather and H. Metiu, Chem. Phys. Lett **157**, 505 (1989).
[19] N. E. Henriksen and E. J. Heller, J. Chem. Phys. **91**, 4700 (1989).
[20] G. W. King and A. W. Richardson, J. Mol. Spectrosc. **21**, 339 (1966).
[21] J. H. Ling and K. R. Wilson, J. Chem. Phys. **63**, 101 (1975).
[22] A. P. Baronavski and J. R. McDonald, Chem. Phys. Lett. **45**, 172 (1977).
[23] W. M. Pitts and A. P. Baronavski, Chem. Phys. Lett. **71**, 395 (1980).
[24] W. Krieger, J. Häger, and J. Pfab, Chem. Phys. Lett. **85**, 69 (1982).
[25] A. P. Baronavski, Chem. Phys. **66**, 217 (1982).
[26] W. H. Fisher, T. Carrington, S. V. Filseth, C. M. Sadowski, and C. H. Dugan, Chem. Phys. **82**, 443 (1983).
[27] I. Nadler, H. Reisler, and C. Wittig, Chem. Phys. Lett. **103**, 451 (1984).
[28] W. H. Fisher, R. Eng, T. Carrington, C. H. Dugan, S. V. Filseth, and C. M. Sadowski, Chem. Phys. **89**, 457 (1984).
[29] W. J. Marinelli, N. Sivakumar, and P. L. Houston, J. Phys. Chem. **88**, 6685 (1984).
[30] F. Shokoohi, S. Hay, and C. Wittig, Chem. Phys. Lett. **110**, 1 (1984).
[31] I. Nadler, D. Mahgerefteh, H. Reisler, and C. Wittig, J. Chem. Phys. **82**, 3885 (1985).
[32] G. E. Hall, N. Sivakumar, and P. L. Houston, J. Chem. Phys. **84**, 2120 (1986).
[33] J. L. Knee, L. R. Khundkar, and A. H. Zewail, J. Phys. Chem. **89**, 4659 (1985).
[34] N. F. Scherer, J. L. Knee, D. D. Smith, and A. H. Zewail, J. Phys. Chem. **89**, 5141 (1985).
[35] H. Joswig, M. A. O'Halloran, R. N. Zare, and M. S. Child, Faraday Discuss. Chem. Soc. **82**, 79 (1986).
[36] W. P. Hess and S. R. Leone, J. Chem. Phys. **86**, 3773 (1987).
[37] M. A. O'Halloran, H. Joswig, and R. N. Zare, J. Chem. Phys. **87**, 303 (1987).
[38] M. Dantus, M. J. Rosker, and A. H. Zewail, J. Chem. Phys. **87**, 2395 (1987).
[39] E. Hasselbrink, J. R. Waldeck, and R. N. Zare, Chem. Phys. **126**, 191 (1988).
[40] M. Dantus, M. J. Rosker, and A. H. Zewail, J. Chem. Phys. **89**, 6128 (1988).
[41] A. Paul, W. H. Fink, and W. M. Jackson, Chem. Phys. Lett. **153**, 121 (1988).
[42] M. J. Rosker, M. Dantus, and A. H. Zewail, J. Chem. Phys. **89**, 6113 (1988).
[43] A. H. Zewail, J. Chem. Soc. Faraday Trans. 2 **85**, 1221 (1989).
[44] J. F. Black, J. R. Waldeck, E. Hasselbrink, and R. N. Zare, J. Chem. Phys. Soc. Faraday Trans. 2 **85**, 1044 (1989).
[45] J. H. Ling and K. R. Wilson, J. Chem. Phys. **65**, 881 (1976).
[46] G. Herzberg, *Molecular Spectra and Molecular Structure I. Spectra of Diatomic Molecules* (Van Nostrand Reinhold, New York, 1950).
[47] J. Weinard, Ann. Astrophys. **18**, 334 (1955).
[48] B. Brocklehurst, G. R. Herbert, S. H. Innanen, R. M. Seel, and R. W. Nichols, *Identification Atlas of Molecular Spectra 9. The CN $B\,^2\Sigma^+ - X\,^2\Sigma^+$ Violet System* (York University Centre for Research in Experimental Space Science, Toronto, 1972).
[49] R. Engleman, Jr., Mol. Spectrosc. **49**, 106 (1974).
[50] D. Cerny, R. Bacis, G. Guelachvili, and F. Roux, J. Mol. Spectrosc. **73**, 154 (1978).
[51] H. Ito, Y. Ozaki, K. Suzuki, T. Kondow, and K. Kuchitsu, J. Mol. Spectrosc. **127**, 283 (1988).
[52] R. N. Dixon, J. Chem. Phys. **85**, 1866 (1986).
[53] M. Dubs, U. Brühlmann, and J. R. Huber, J. Chem. Phys. **84**, 3106 (1986).
[54] G. E. Hall, N. Sivakumar, P. L. Houston, and I. Burak, Phys. Rev. Lett. **56**, 1671 (1986).
[55] G. E. Hall, N. Sivakumar, D. Chawla, P. L. Houston, and I. Burak, J. Chem. Phys. **88**, 3682 (1988).
[56] M. P. Docker, Chem. Phys. **135**, 405 (1989).
[57] J. R. Waldeck, J. F. Black, and R. N. Zare (unpublished work); J. R. Waldeck, Ph.D. thesis, Stanford University, Stanford, Calif. 1989.
[58] Figures 3–17 were generated using the PLT2 plotting package, written jointly by individuals at the Department of Chemistry, Harvard University, Cambridge, Mass., and the Cardiac Unit, Massachusetts General Hospital, Boston, Mass.
[59] R. N. Zare, Ph.D. thesis, Harvard University, Cambridge, Mass., 1964.
[60] R. N. Zare and D. R. Herschbach, Proc. IEEE **51**, 173 (1963).
[61] J. Solomon, J. Chem. Phys. **47**, 889 (1967).
[62] G. E. Busch and K. R. Wilson, J. Chem. Phys. **56**, 3638 (1972).
[63] C. Jonah, J. Chem. Phys. **55**, 1915 (1971).
[64] T. Nagata, T. Kondow, K. Kuchitsu, G. W. Loge, and R. N. Zare, Mol. Phys. **50**, 49 (1983); T. Nagata, T. Kondow, and R. N. Zare (in preparation).
[65] R. Schmiedl, H. Dugan, W. Meier, and K. H. Welge, Z. Phys. A **304**, 137 (1982).
[66] R. Bersohn and S. Lin, Adv. Chem. Phys. **16**, 67 (1969).
[67] S. Yang and R. Bersohn, J. Chem. Phys. **61**, 4400 (1974).
[68] S. E. Choi and R. B. Bernstein, J. Chem. Phys. **85**, 150 (1986).
[69] R. N. Zare, *Angular Momentum* (Wiley, New York, 1988).
[70] R. N. Zare, Mol. Photochem. **4**, 1 (1972).
[71] G. E. Busch and K. R. Wilson, J. Chem. Phys. **56**, 3626 (1972).
[72] G. N. A. van Veen, T. Baller, A. E. de Vries, and N. J. A. van Veen, Chem. Phys. **87**, 405 (1984).
[73] M. D. Barry and P. A. Gorry, Mol. Phys. **52**, 461 (1984) and references therein.
[74] R. E. Continetti, B. A. Balko, and Y. T. Lee, J. Chem. Phys. **89**, 3383

(1988).
[75] R. O. Loo, H.-P. Haerri, G. E. Hall, and P. L. Houston, J. Chem. Phys. **90**, 4222 (1989).
[76] D. W. Chandler, J. W. Thoman, M. H. M. Janssen, and D. H. Parker, Chem. Phys. Lett. **156**, 151 (1989).
[77] M. Mons and I. Dimicoli, J. Chem. Phys. **90**, 4037 (1989).
[78] I. Powis and J. F. Black, J. Phys. Chem. **93**, 2461 (1989).
[79] Numerical Algorithms Group, NAG, Inc., Downers Grove, Ill.
[80] P. E. Gill, W. Murray, and M. H. Wright, *Practical Optimization* (Academic, London, 1981).
[81] P. R. Bevington, *Data Reduction and Error Analysis for the Physical Sciences* (McGraw–Hill, New York, 1969).
[82] J. F. Black and R. N. Zare (in preparation).
[83] R. I. Altkorn, R. N. Zare, and C. H. Greene, Mol. Phys. **55**, 1 (1985).
[84] J. A. Guest, M. A. O'Halloran, and R. N. Zare, Chem. Phys. Lett. **103**, 261 (1984).
[85] P. M. Morse and H. Feshbach, *Methods of Theoretical Physics* (McGraw–Hill, New York, 1953).
[86] G. Cazzoli, C. Degli-Esposti, and P. G. Favero, J. Mol. Struct. **48**, 1 (1978).
[87] S. Carter, I. M. Mills, and R. N. Dixon, J. Mol. Spectrosc. **106**, 411 (1984).
[88] M. S. Child, Mol. Phys. **16**, 313 (1971).
[89] C. J. Williams, K. F. Freed, S. J. Singer, and Y. B. Band, Faraday Discuss. Chem. Soc. **82**, 51 (1986) and references therein.
[90] S. J. Singer, K. F. Freed, and Y. B. Band, Adv. Chem. Phys. **61**, 1 (1985).
[91] K. F. Freed and Y. B. Band (private communication).
[92] J. F. Black, E. Hasselbrink, J. R. Waldeck, and R. N. Zare (in preparation).
[93] J. F. Black, J. R. Waldeck, and R. N. Zare, J. Chem. Soc. Faraday Trans. 2 **85**, 1312 (1989).
[94] J. W. Rabalais, J. M. McDonald, V. Scherr, and S. P. McGlynn, Chem. Rev. **71**, 73 (1971).
[95] J. F. Black and I. Powis, Chem. Phys. **125**, 375 (1988), and references therein.
[96] M. Shapiro, J. Phys. Chem. **90**, 3644 (1986).
[97] K. Q. Lao, M. D. Person, P. Xayariboun, and L. J. Butler, J. Chem. Phys. **92**, 823 (1990).
[98] S. Yabushita and K. Morokuma, Chem. Phys. Lett **153**, 517 (1988).
[99] M. Tadjeddine, J. P. Flament and C. Teichteil, Chem. Phys. **118**, 45 (1987).
[100] R. N. Dixon, Mol. Phys. **68**, 263 (1989).
[101] M. P. Docker, A. Hodgson, and J. P. Simons, Faraday Discuss. Chem. Soc. **82**, 25 (1986).
[102] S. Klee, K.-H. Gericke, and F. J. Comes, J. Chem. Phys. **85**, 40 (1986).
[103] K.-H. Gericke, S. Klee, F. J. Comes, and R. N. Dixon, J. Chem. Phys. **85**, 4463 (1986).
[104] A. E. Bruno, U. Brühlmann, and J. R. Huber, Chem. Phys. **120**, 155 (1988).
[105] A. Ticktin, A. E. Bruno, U. Brühlmann, and J. R. Huber, Chem. Phys. **125**, 403 (1988).
[106] Y. Y. Bai, A. Ogai, C. X. W. Qian, L. Iwata, G. A. Segal, and H. Reisler, J. Chem. Phys. **90**, 3903 (1989).
[107] C. H. Greene and R. N. Zare, J. Chem. Phys. **78**, 6741 (1983).
[108] N. Sivakumar, G. E. Hall, P. L. Houston, J. W. Hepburn, and I. Burak, J. Chem. Phys. **88**, 3692 (1988).